Roughness-Induced Boundary Layer Transition

by

Margaret Elizabeth Grimaldi

Submitted to the Department of Aeronautics and Astronautics
in partial fulfillment of the requirements for the degree of

Master of Science in Aeronautics and Astronautics

at the

MASSACHUSETTS INSTITUTE OF TECHNOLOGY

May 1994

Author_____
Department of Aeronautics and Astronautics
May 11, 1994

Certified by_____
Professor Kenneth S. Breuer
Assistant Professor
Thesis Supervisor

Accepted by_____
Professor Harold Y. Wachman
Chairman, Departmental Committee on Graduate Students

Roughness-Induced Boundary Layer Transition

by

Margaret Elizabeth Grimaldi

Submitted to the Department of Aeronautics and Astronautics
on May 11, 1994, in partial fulfillment of the
requirements for the degree of
Master of Science in Aeronautics and Astronautics

Abstract

Two-dimensional roughness effects on flat plate boundary layer transition were investigated. Receptivity, associated with the generation of instabilities in the boundary layer, was addressed in three-element roughness array experiments at amplitudes of $0.12mm$, $0.24mm$, and $0.36mm$. Instability generation was maximized by centering the roughness array at branch I of the neutral stability curve for a selected frequency and tuning the roughness spacing with the instability wavelength at branch I. Results show a linear relationship between an increase in boundary layer receptivity and an increase in roughness height for all roughness amplitudes in this configuration. Resonant nonlinear interactions were observed in the resulting velocity spectra through the appearance of harmonics. Transition occurs earlier than for a smooth plate with an increase in roughness amplitude and in a manner predicted by linear stability theory. Mean flow distortion resulting from large-amplitude roughness was addressed in single-element roughness experiments. Roughness heights of $0.72mm$, $0.96mm$, and $1.20mm$ were investigated. The mean flow recovers quickly from the inflectional instability caused by separation off the lower amplitude roughness elements. However, the largest amplitude roughness element generates a severely inflected mean flow profile which does not recover prior to transition. In all cases, mean flow distortion was observed and transition occurred with decreasing distance downstream of the roughness as the roughness amplitude was increased. The path to transition occurred through amplification of high frequency bands rather than amplification of instability waves associated with linear theory. Results also show an influence of the Reynolds number on the transition process.

Thesis Supervisor: Professor Kenneth S. Breuer
Title: Assistant Professor

Acknowledgments

I was fortunate to have been offered the opportunity to conduct this research through Professor Kenny Breuer with funding from the National Science Foundation. Kenny's knowledge and energy guided the technical accomplishments presented in this thesis. His efforts in the laboratory were vital in establishing the tools necessary to conduct this research, making things much less difficult for me. I am grateful for all that I have learned from him and for the patience he has demonstrated on many occasions over the last year and a half.

I would like to thank my family and friends who have endured and supported me since I arrived at M.I.T. Both helped to make my experience more pleasant and rewarding. I want to thank Errol Arkilic for always having something positive to say during the not so productive days in the lab and in the writing of this thesis. I especially want to thank Ruben Rathnasingham with whom I shared all of the difficult times and moments of comic relief in the lab. Things would not have been the same without him. I don't know if he became my friend just because I could spell his last name right, but I am grateful for his friendship and to have had the opportunity to learn from him.

Finally, I would like to thank John Dzenitis. His continual support and care during this time helped me to succeed while keeping in focus the important things in life.

Contents

List of Figures

List of Tables

Chapter 1

Introduction

The desire to better understand boundary layer transition has motivated studies on this subject for over a century. Flows in which the presence of a turbulent boundary layer can prove detrimental or in which the location of transition is important have given cause for experimental and theoretical efforts to identify mechanisms influencing the change from laminar to turbulent flow. Surface roughness, commonly encountered in real flow situations, poses a problem which requires a better understanding of two such mechanisms–scattering of external acoustic waves and distortion of the mean flow by large roughness elements.

The intent of this chapter is to provide an introduction to the theories and experimental work leading to the present research in which these mechanisms are investigated.

1.1 Small Disturbance Amplification and Surface Roughness

Growth and decay of small disturbances in a smooth plate, laminar boundary layer is predicted by linear stability theory through the solution of the Orr-Sommerfeld equation. These disturbances take the form of travelling Tollmein-Schlichting (T-S) instability waves which may eventually lead to boundary layer transition. Instability

mechanisms which influence this selective amplification process or the initial disturbance amplitude can bring about early transition.

Surface roughness introduces two instability mechanisms which are of interest in this research: receptivity and mean flow distortion. Each is different in its effect on disturbance amplification. Receptivity describes the generation of instability waves in the boundary layer, whereas mean flow distortion provides a mechanism for broadband amplification of high-frequency disturbances, often outside of the T-S band of instabilities.

1.1.1 Receptivity

Receptivity, as defined by Kerschen [8], is " the process by which external disturbances generate instability waves in the boundary layer". If the external disturbances are in the form of acoustic waves, the freestream fluctuations have wavelengths several orders of magnitude larger than the instability wavelengths. Energy is transferred from the acoustic waves to the T-S instabilities through wavelength scattering. Scattering can occur where the boundary layer is forced to make a rapid adjustment as would result from surface inhomogeneities. The small length scale associated with the inhomogeneity is transferred to the larger wavelength disturbances in the outer flow. The resulting scattered waves are then of a scale which is able to interact with other instabilities in the boundary layer [3].

Receptivity experiments performed by Saric *et al.* [11] and Wiegel and Wlezien [13] have demonstrated wavelength scattering and instability generation. Strips of roughness located at branch I of the neutral stability curve for a selected T-S wave frequency resulted in the generation of instabilities at this frequency which immediately begin to amplify. Branch I corresponds to the Reynolds number location where disturbance amplification begins. Locating the roughness at this location results in maximum initial energy of the instabilities which have no time to decay prior to beginning the amplification process.

A detuning mechanism is present in the case of surface waviness or multiple roughness elements. This was investigated theoretically by Crouch [6] and demonstrated

experimentally by Wiegel and Wlezien [13]. The effect of matching the forced mode parameters with the T-S parameters is to cause a resonance between the forcing and the eigenmode solution [6]. When the wavenumber associated with the surface roughness no longer corresponds to the T-S wavenumber at that location, detuning is observed through reduced instability amplification.

Increased generation of instabilities through receptivity provides an opportunity for greater interaction between disturbances. As these disturbances amplify, earlier transition to turbulence can result.

1.1.2 Distorted Mean Flow Instability

Roughness elements of sufficient amplitude can cause distortion of the mean flow. When this is the case, the dominant instability mechanism is no longer associated with linear theory as was discussed for receptivity.

Experiments which have produced evidence of the mean flow distortion effect were performed by Klebanoff and Tidstrom [9] using 2-D roughness elements. The roughness parameter k/δ_k^*, where k is the roughness height and δ_k^* is the displacement thickness at the roughness location in the undisturbed flow, was sufficiently large to establish an inflection in the mean flow profile. Downstream of the roughness element, transition occurred in a manner similar to that for a smooth plate, but with decreasing Reynolds number as the roughness ratio was increased.

Unlike the amplification of T-S waves found with small scale roughness, amplified disturbances consist of high frequencies which may lie outside of the T-S wave frequency range. The most amplified frequency shifts to lower values as the distance downstream increases. However, transition often occurs without the selective amplification process defined by linear stability theory. In cases where an inflectional profile exists and T-S instabilities are amplified, Klebanoff and Tidstrom [9] found there to be greater amplification of the instability than would result for a smooth plate.

The geometric factors which influence the shape of the velocity profile and thus the stability of the flow are the height to width ratio, k/b, and the roughness location,$R_{\delta_k^*}$. This was demonstrated experimentally by Klebanoff and Tidstrom [9] and theoreti-

cally by Nayfeh *et al.* [10].

1.2 Present Work

In past experiments which were discussed in relation to receptivity and mean flow distortion, a clear distinction exists between the investigated roughness heights and the resulting mechanism affecting boundary layer stability. The purpose of the present research is to investigate a range of roughness heights between these extremes $0.04mm \leq k \leq 1.68mm$ $(0.032 \leq k/\delta_k^* \leq 0.86)$ and to characterize the destabilizing mechanisms which lead to transition.

In these investigations, relative amplitudes of excited T-S waves as well as broad-band high frequency amplification are of interest. Precise transition location is not the goal as much as understanding the effects of various roughness parameters in producing earlier transition.

Receptivity as a function of roughness parameters will be investigated for linear relationships similar to the work of Saric [11] and Wiegel and Wlezien [13] with the focus on natural disturbances in the environment rather than externally forced acoustic disturbances. The advantage of a more realistic, naturally excited environment is that all frequencies are of comparable amplitude allowing a broad range of nonlinear interactions to be observed. The disadvantage is that linear interactions which are predicted by theory may not be well observed.

The effect of roughness height on the mean flow will be considered in an effort to identify the amplitudes associated with the mean flow distortion mechanism. Deviation from smooth plate profiles as well as other roughness levels will be investigated.

Chapter 2

Experimental Setup and Techniques

All experiments supporting this research were performed in the Low Turbulence Wind Tunnel Laboratory in the department of Aeronautics and Astronautics at the Massachusetts Institute of Technology.

2.1 Wind Tunnel and Flat Plate

The primary apparatus used to support this research was an open circuit, low turbulence wind tunnel shown in Figure 2-1. The tunnel is comprised of a 16:1 contraction, followed by a $0.61m \times 0.91m \times 3.66m$ interchangeable test section, diffuser, motor and fan. The x-direction is defined as positive downstream, the y-direction is normal to the vertical doors of the test section, and the z-direction is positive toward the floor from the test section centerline.

Several flow straightening devices were installed at the inlet to improve the quality of flow entering the test section. Bell shaped surfaces were included on three sides of the inlet help to reduce inlet separation, and a $0.10m$ thick honeycomb followed by four seamless screens spaced $0.14m$ apart inside of the contraction reduce longitudinal and lateral velocity fluctuations. The resulting freestream turbulence level in the test section was measured to be less than 0.08 percent in the streamwise direction at

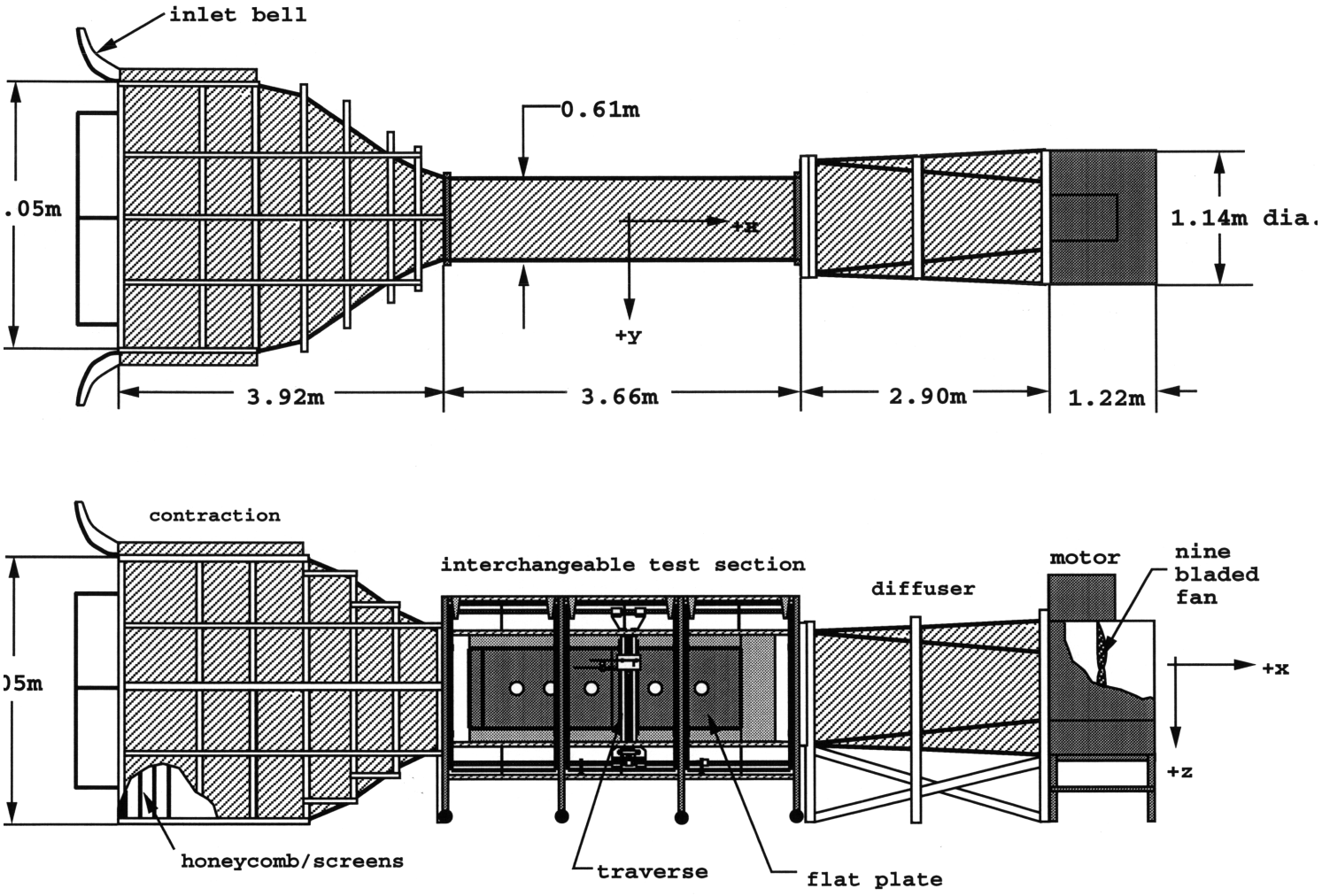

Figure 2-1: Low Turbulence Wind Tunnel. Department of Aeronautics and Astronautics, M.I.T.

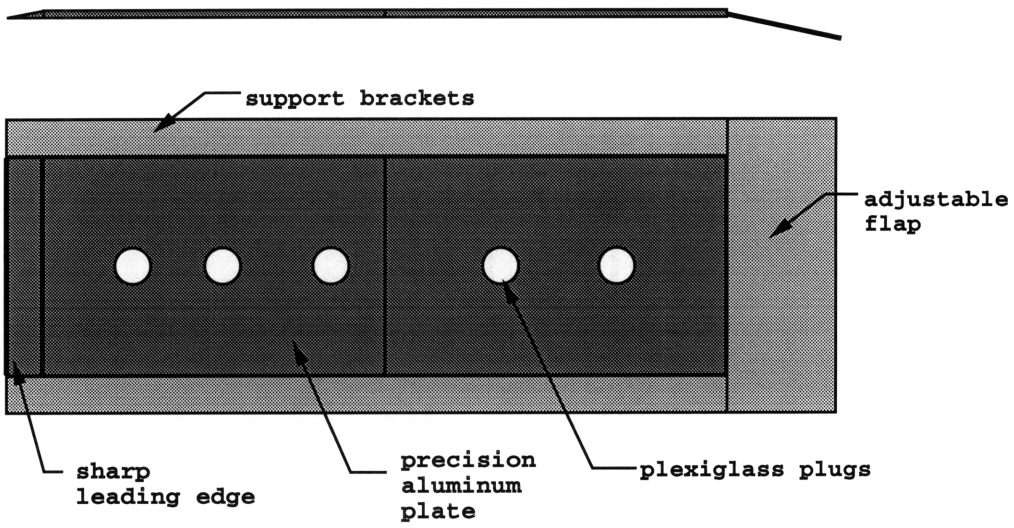

Figure 2-2: Flat Plate $2.5m \times 0.74m \times 0.0095m$.

$12.5m/s$. Freestream velocities up to $20m/s$ can be comfortably achieved in the test section.

A flat plate constructed from two precision aluminum plates joined along the width was installed in the test section (Figure 2-2). A sharp leading edge extension $0.10m$ in length was attached to the front end of the plate with a wedge angle of approximately 10 degrees opening toward the nonworking side. A trailing edge flap $0.50m$ in length was attached to the opposite end of the plate. The adjustable flap was used to move the stagnation point to the working side of the plate. The resulting plate dimensions, excluding the flap, were approximately $2.50m \times 0.74m \times 0.01m$. Forty-two pressure taps were installed along the length of the plate, twenty-two on each side of the centerline, to provide pressure gradient information. Five plexiglass plugs were also installed at various locations along the centerline for experiments unrelated to this research. All seams were filled with putty and sanded smooth.

The flat plate was positioned vertically in the test section $0.50m$ from the entrance and fastened to the floor and ceiling with support brackets along its length (Figure 2-3). The leading edge was placed between the tunnel centerline and the far wall with a downstream diverging angle of approximately 0.30 degrees. This orientation was

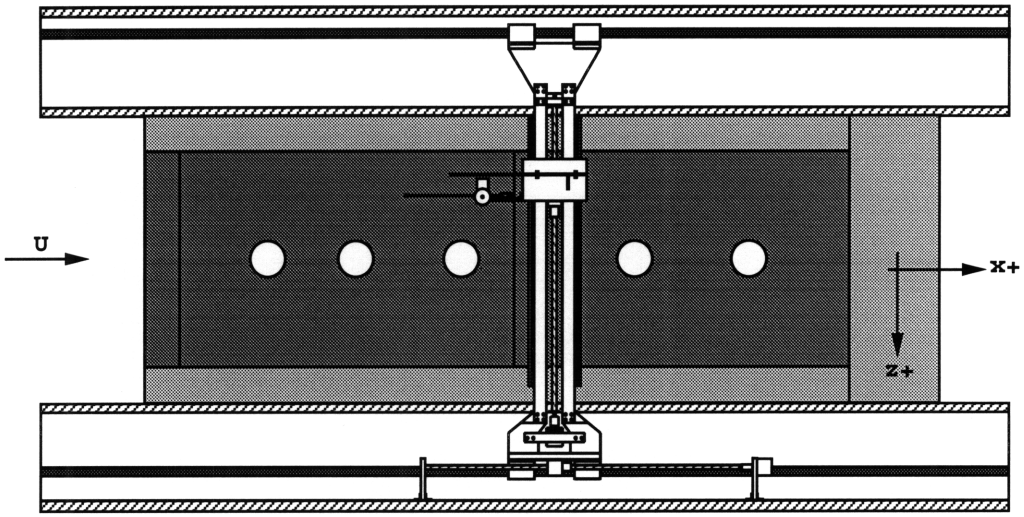

Figure 2-3: Interchangeable Test Section $0.61m \times 0.91m \times 3.66m$.

selected based on shape factor results and pressure readings along the plate. A flap angle of approximately 10 degrees was necessary to set the leading edge attachment and to minimize the pressure gradient.

A turbulent boundary layer develops on the walls of the tunnel producing a contamination zone in the test section. The extent of the contamination zone was measured at $12.5m/s$ with the flat plate installed and found to increase at an angle of approximately 10 degrees downstream, beginning at the entrance to the test section, until full contamination was present $2.50m$ from the entrance.

2.2 Traverse

A stepper-motor-driven, programmable, three-axis traversing mechanism was installed in the test section for precise and automatic placement of flow measuring instrumentation (Figure 2-4). The x-traverse provides travel up to $0.50m$ with $0.007mm$ resolution and can be moved to any streamwise portion of the test section where measurements are to be made. If the desired range of measurements exceeds $0.50m$, the main traversing structure can be disconnected from the x-traverse and positioned

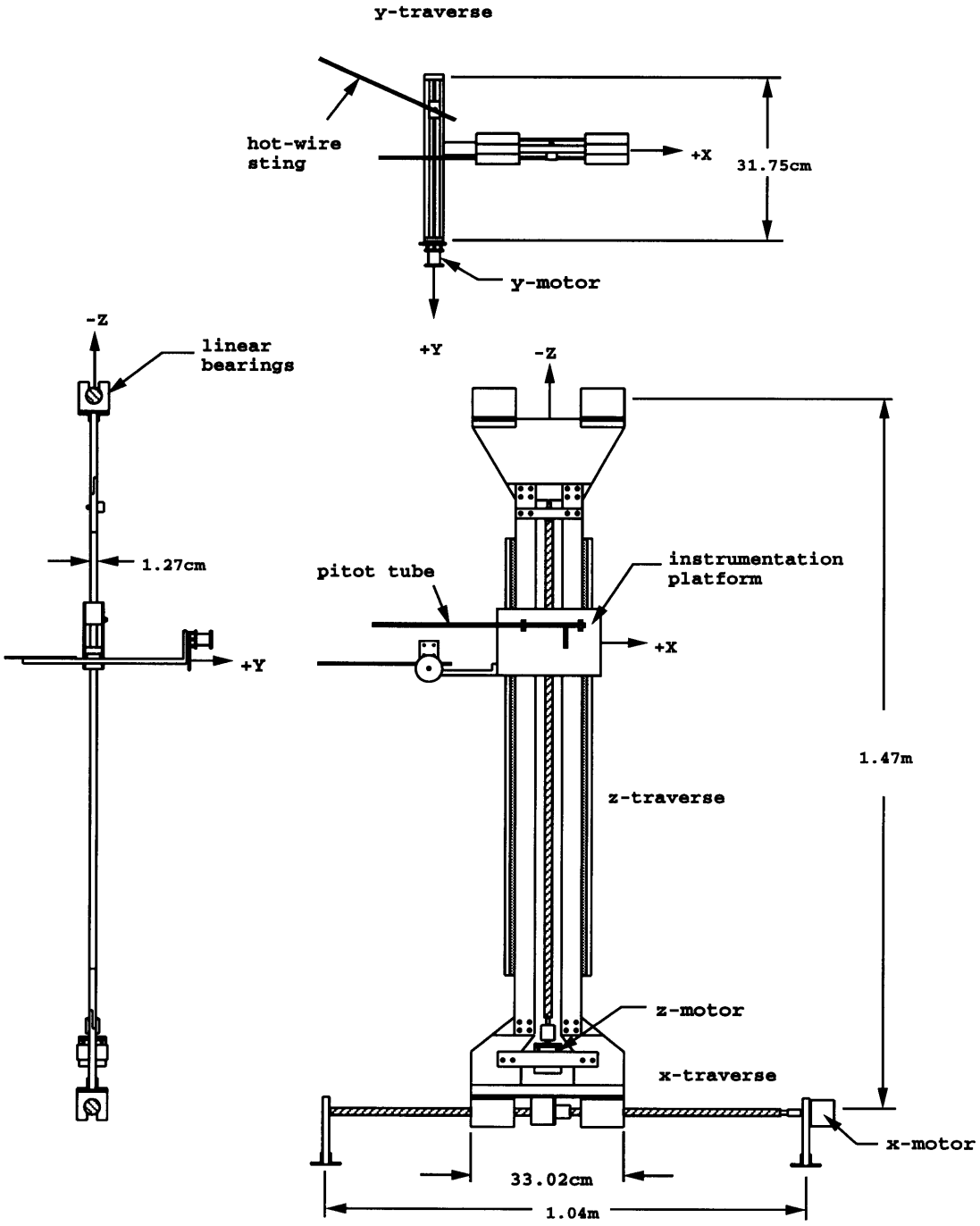

Figure 2-4: Three-Dimensional Wind Tunnel Traverse.

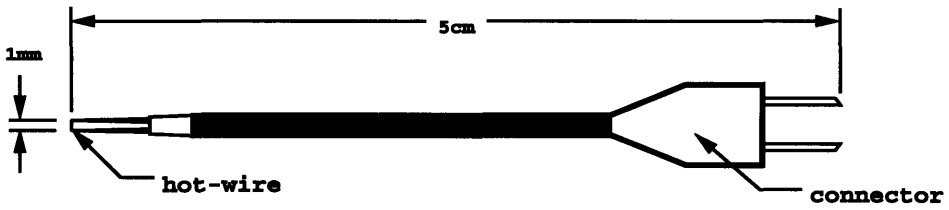

Figure 2-5: Hot-wire Probe.

manually. The y-traverse provides positioning up to $0.10m$ normal to the flat plate and is geared to give $0.004mm$ resolution. The z-traverse can position the instrumentation platform up to $0.26m$ on either side of the tunnel centerline with $0.007mm$ resolution.

2.3 Instrumentation and Data Acquisition

A custom built, constant temperature hot-wire anemometer was used for measuring flow velocity in the streamwise direction. A $10kHz$ frequency response was more than adequate for the measurements of interest on the order of $1kHz$. Four gain settings between 1 and 96 were available which enabled the output voltage to range between ± 10 volts, matching the input range of the A/D converter.

Hot-wire probes were constructed in the laboratory. The hot-wire is a single $2.54\mu m$ diameter platinum-rhodium wire, $1mm$ in length, welded between two prongs (Figure 2-5). The overall length of a probe was approximately $5cm$ and was mounted to the end of a $25cm$ long carbon fiber sting on the y-traverse through a connector inside of the sting. The length of the sting was sufficient to place the probe out of the disrupted flow near the traverse.

Each probe was calibrated prior to a test series. Anemometer voltages were calibrated with pressure transducer voltages using a cubic polynomial calibration method. Eight velocity settings between $0.85m/s$ and $15m/s$ were sampled and the resulting curve fit was off by no more than one percent for each calibration. Drift from the

calibrated velocities was checked periodically and the probe was recalibrated when necessary.

Data acquisition and reduction were performed using a Gateway 2000-486 personal computer. A 16-channel, 12-bit A/D converter installed in the computer was used to digitize anemometer and Baratron output voltages with 0.0049 volt resolution. The computer was also used to command the traverse stepper motors.

Most of the computer programs used for this research were written in C. Some programming was done in Matlab for analyzing and plotting the results.

2.4 Experimental Procedure

Prior to starting an experiment, the probe was calibrated as described in section 2.3. The anemometer was set to an overheat ratio of 1.31 and a filter setting of $10kHz$. A program written for automatic probe positioning and data acquisition was then executed. The traversing sequence could include streamwise (x), spanwise (z) and boundary layer (y) traversing depending upon the user input. A starting location in the boundary layer was determined by specifying a fraction of the freestream velocity using the pitot tube velocity as a reference.

Most spectra presented in this thesis were measured at a y-location corresponding to $U/U_o = 0.15$ where U is the velocity in the boundary layer and U_o is the freestream velocity. Although this does not correspond to the location of maximum T-S wave amplitude, which is closer to $U/U_o = 0.30$, all of the features that characterize this mode of transition are clearly observed. In some cases such as harmonic generation, $U/U_o = 0.15$ gives a clearer picture of the velocity spectrum. Some important observations which were made at $U/U_o = 0.30$ will be discussed in Chapter 4 in relation to the generation of subharmonics.

After the boundary layer was traversed, a least squares fit of the data in the linear region of the near wall laminar velocity profile was used to determine the actual starting distance from the plate. In cases where the velocity profile contained a non-linear region near the wall, a shift in y-location was performed to match theoretical

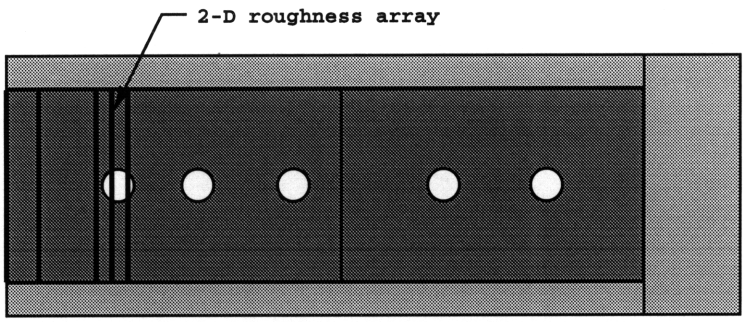

Figure 2-6: Flat plate with a two-dimensional roughness array.

results near the edge of the boundary layer. In cases where only one position was measured in the boundary layer, the y-location was determined based on the probe positioning data which was collected while locating the desired starting velocity. All experiments were run at a velocity of $12.5m/s$.

2.5 Roughness

All two-dimensional roughness elements were constructed from $0.12mm$ thick by $4.23mm$ wide Maco brand tape. Desired roughness heights were achieved through lamination and spanned the entire width of the plate either as a single element or in an array of three elements as shown in Figure 2-6. Roughness height could vary along the span by $\pm 0.013mm$ for the arrays and $\pm 0.050mm$ for large amplitude single elements. Location and spacing of the roughness was determined from stability theory and will be discussed in Section 4.2.

Chapter 3

Characterization of the Smooth Plate Boundary Layer

Characterization of the flow over a smooth plate was performed by measuring boundary layer velocity profiles and velocity spectra at various streamwise and spanwise locations on the plate. Results were compared with Blasius and Falkner-Skan solutions and later to experimental roughness results.

3.1 Mean Flow Profiles

Boundary layer velocity profiles were measured every $0.20m$ along the flat plate between $x = 0.30m$ and $x = 1.70m$ at $U_o = 12.5m/s$. Laminar flow was observed along the centerline up to $1.80m$, beyond which transition occurred due to sidewall contamination. A minimum of 30 locations in the y-direction were measured between the plate and the freestream with variable spacing to provide increased resolution near the wall. The parameter η is the nondimensional measure of distance from the plate defined by $\eta = y\sqrt{\frac{U_o}{\nu x}}$.

Figure 3-1 shows the resulting experimental data plotted with a zero virtual origin. These profiles were found to match a Falkner-Skan profile with $\beta = 0.0155$ (wedge angle of 0.048 degrees), indicating the existence of a slightly favorable pressure gradient along the plate. Pressure coefficient measurements along the plate support this

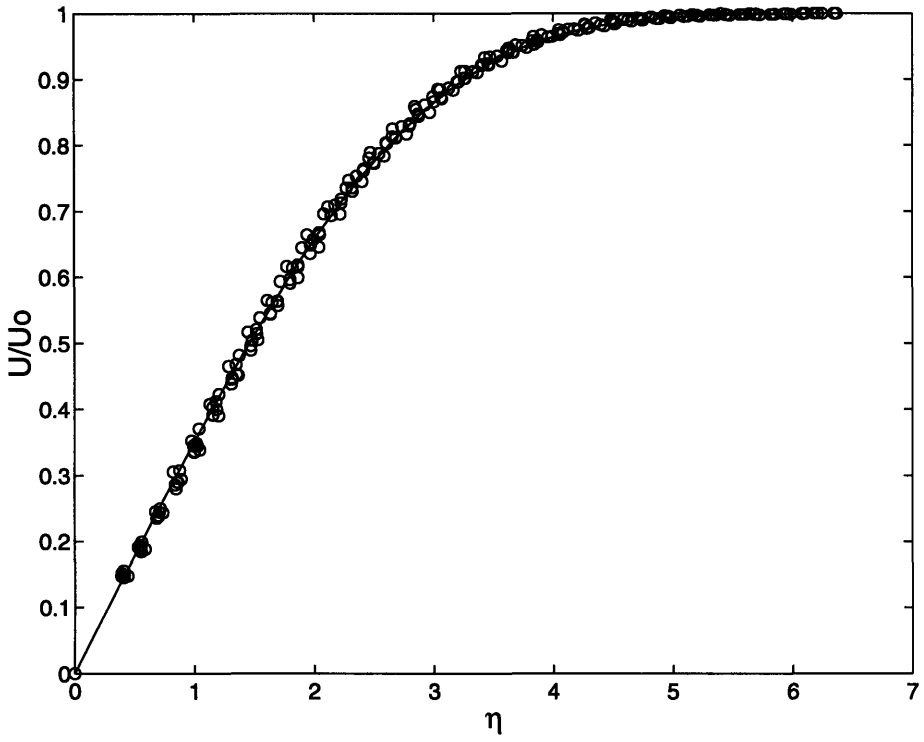

Figure 3-1: Experimental mean flow data (o) versus Falkner-Skan $\beta = 0.0155$ (-), $U_o = 12.5m/s$. Measurements taken at centerline locations $x = 0.30m$ to $1.70m$.

result where $C_p = (P - P_{ref})/(P_o - P_{ref})$. P is the static pressure at the location of interest, P_{ref} is the reference static pressure, and P_o is the total pressure. Shape factor measurements did not reflect an obviously favorable gradient. However, due to the sensitivity in calculating the displacement and momentum thickness, it is likely that a slight error in these measurements is the cause of the discrepancy.

Deviation of the experimental mean flow results from the Falkner-Skan solution at selected streamwise locations are shown in Figure 3-2. The experimental results appear to deviate from Falkner-Skan by approximately one percent for $R_{\delta^*} = 1080$ and the deviation increases to three percent downstream. This may be explained by a spanwise variation in the flow discussed in the following paragraph. The deviation results appear to oscillate about the curve fit, but since a low order polynomial was used, it is believed to be random scatter around a trend. A Reynolds number based

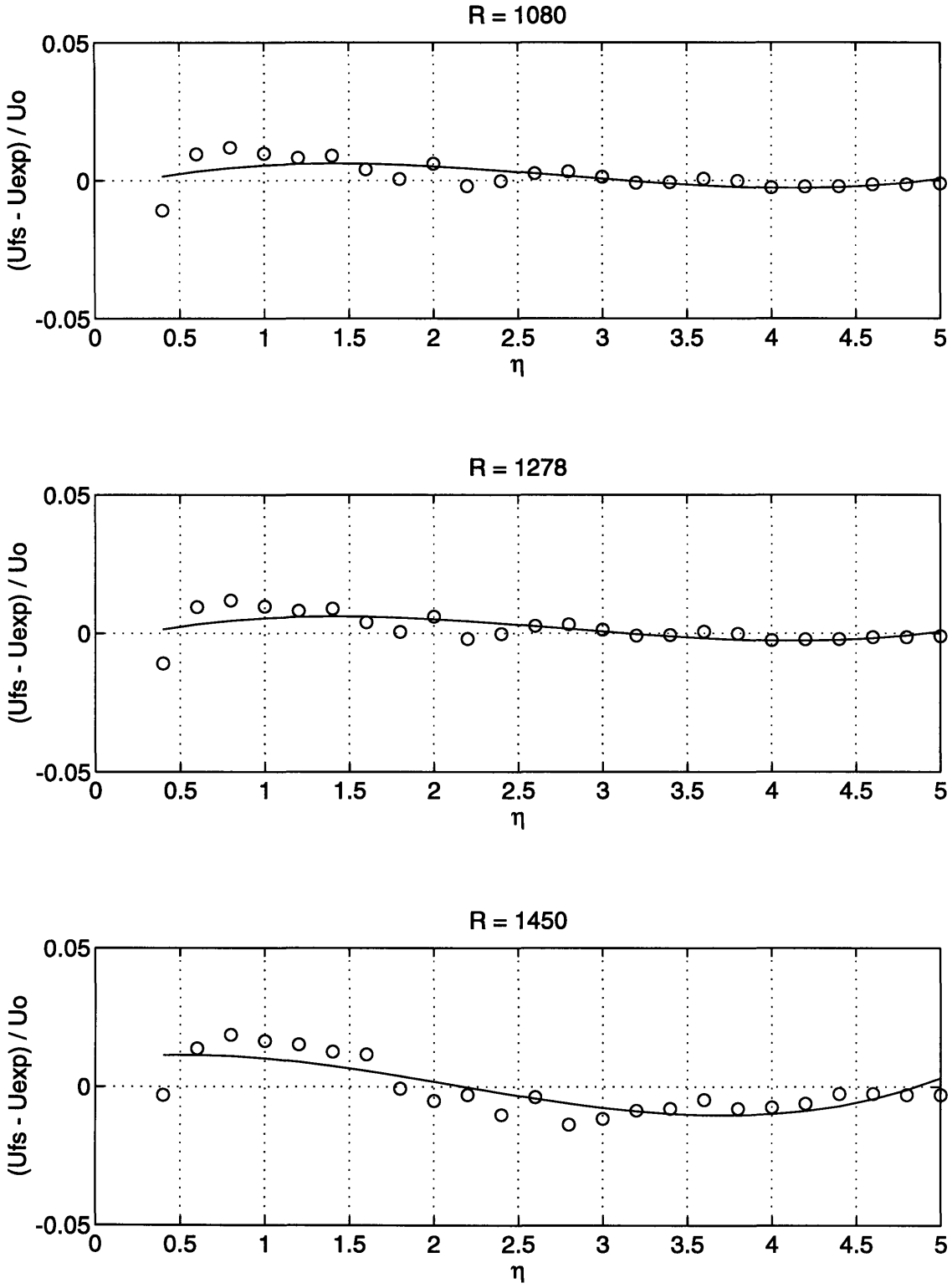

Figure 3-2: Deviation of experimentally measured mean flow from Falkner-Skan $\beta = 0.0155$. $U_{fs} \equiv$ Falkner-Skan velocity, $U_{exp} \equiv$ experimentally measured velocity. $U_o = 12.5m/s$, $R_{\delta^*} = 1080$, 1278, and 1450 ($x = 0.50m$, $0.70m$, and $0.90m$). Solid line represents a third order polynomial curve fit.

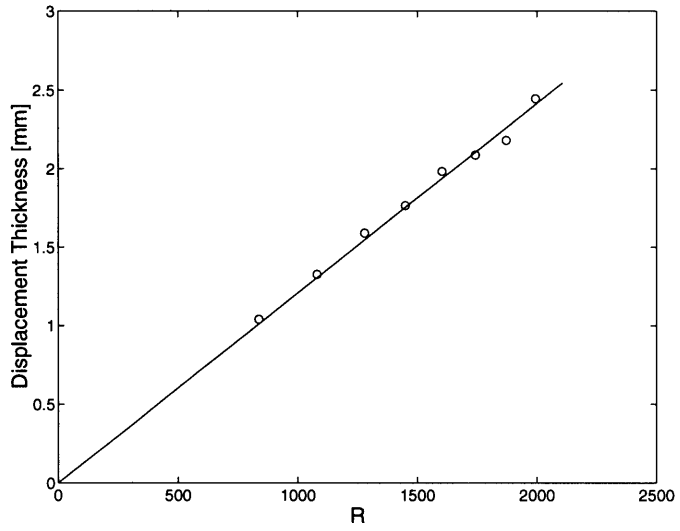

Figure 3-3: Spanwise averaged experimental displacement thickness (o) and Falkner-Skan $\beta = 0.0155$ (-) versus R_{δ^*}, $U_o = 12.5m/s$.

on displacement thickness is defined as $R_{\delta^*} = 1.68\sqrt{\frac{U_o x}{\nu}}$ for a Falkner-Skan profile of $\beta = 0.0155$.

Spanwise variation in the displacement thickness, $\delta^* = 1.68\sqrt{\frac{x\nu}{U_o}}$, was investigated at the same streamwise locations selected for the velocity profiles (Figure 3-3). The extent of the spanwise distance measured at each streamwise location was limited by tunnel wall contamination producing fewer measurements at the downstream locations. The displacement thickness was calculated from the measured profiles using a trapezoidal integration scheme. All spanwise results for each streamwise location were within ten percent of the theoretical Falkner-Skan value. The average displacement thickness across the span was within five percent of the theoretical value. At spanwise locations of $\pm 0.08m$, a reduced displacement thickness was consistently measured downstream of $x = 0.50m$. The low values might be attributed to the existence of pressure ports near these locations.

3.2 Velocity Spectra

3.2.1 Freestream Disturbance Environment

The velocity spectrum shown in Figure 3-4 is representative of the freestream disturbance environment in the experimental facility. The only peaks of significance are found at very low frequencies, associated with the traverse, and near $120Hz$, associated with the natural vibration of the hot-wire sting. The measured disturbance level was less than 0.08 percent of the freestream velocity at $12.5m/s$.

3.2.2 Streamwise and Spanwise Boundary Layer Spectra

Boundary layer velocity spectra for the smooth plate were taken at the same streamwise locations measured for the velocity profiles. The spectrum at $x = 1.0m$, $U/Uo = 0.15$ is shown in Figure 3-5 with the power density normalized by the square of the freestream velocity. This figure displays some features which will be present in all spectra for smooth and rough experiments. The origin of features which can be identified is discussed below.

Frequencies between 1 and $50Hz$ exhibiting high power densities are mainly associated with traverse vibration. The natural frequency of the traverse structure was computed and verifies that these low frequency oscillations are associated with the structure motion and are not flow related. An attempt was made to reduce the low frequency amplification by damping the traverse, but this resulted in a slightly less amplified band shifted to higher frequencies. The shifted band fell in a region of interest to this research and therefore damping was not used. A less stiff method of damping could be developed to eliminate this problem but was not pursued.

A high amplitude band (relative to the noise floor) can be observed between $60Hz$ and $150Hz$ which is composed of several elements. There is a contribution of energy from the T-S instability waves which exist in this range of frequencies. Additionally, a peak in power density can be seen near $120Hz$ associated with the natural frequency of the hot-wire sting. A fan blade passage frequency, calculated to be approximately

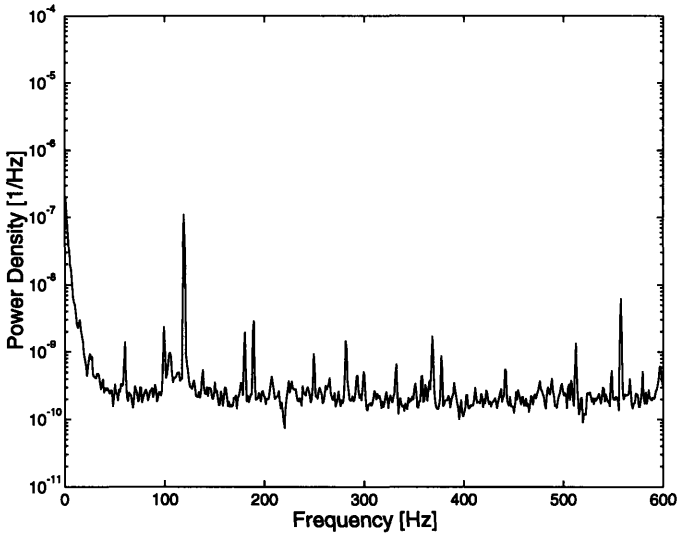

Figure 3-4: Freestream velocity spectrum at $U_o = 12.5m/s$. Power density normalized by U_o^2.

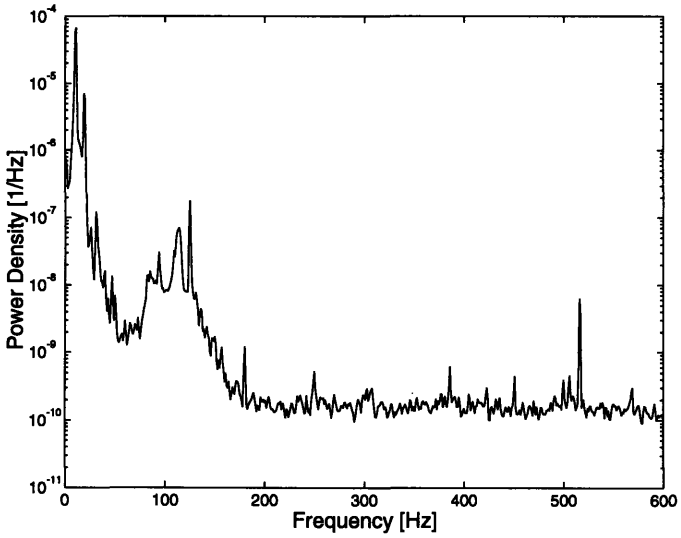

Figure 3-5: Smooth plate velocity spectrum at $R_{\delta^*} = 1528$ ($x = 1.00m$), $U/U_o = 0.15$, $U_o = 12.5m/s$. Power density normalized by U_o^2.

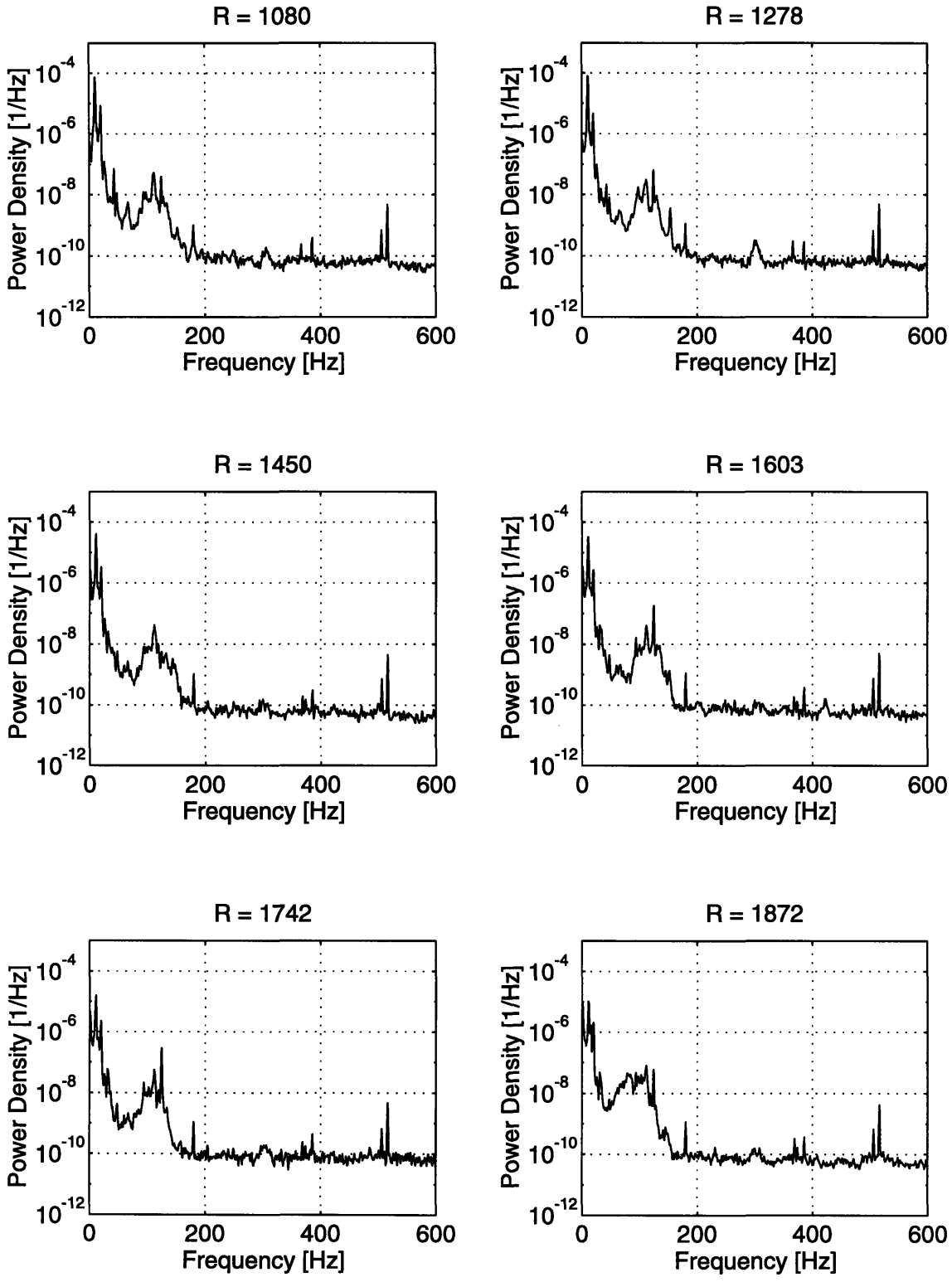

Figure 3-6: Smooth plate centerline velocity spectra with increasing streamwise location, $U/U_o = 0.15$, $U_o = 12.5m/s$. Reynolds number based on displacement thickness. Power density normalized by U_o^2.

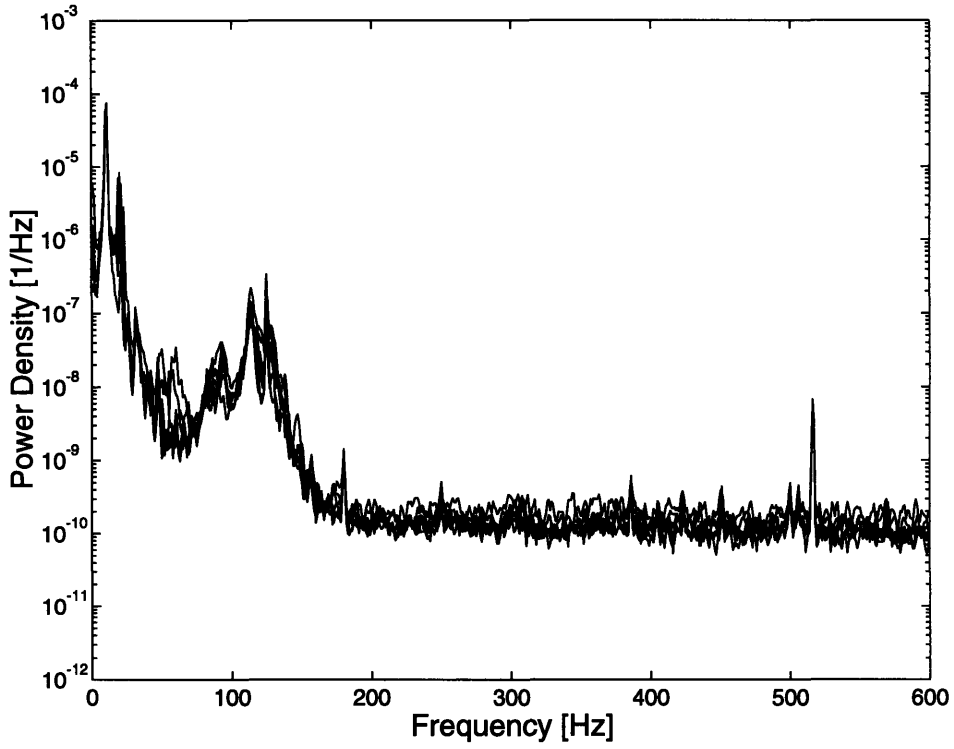

Figure 3-7: Smooth plate spanwise velocity spectra at $R_{\delta^*} = 1528$ ($x = 1.0m$), $U/U_o = 0.15$, $U_o = 12.5m/s$. Spanwise measurements at $z = -0.135m$ to $0.135m$. Power density normalized by U_o^2.

$124Hz$, can also be seen as a sharp peak in this band.

A floor in the spectrum on the order of $10^{-10}/Hz$ exists due to electrical noise in the facility. Measurements of power density below the noise floor could not be made. Repeatability of the measured spectra was good if one was careful to avoid running experiments when external noise levels were unusually high.

Streamwise spectra measured along the plate centerline between $x = 0.50m$ and $x = 1.50m$, $U/U_o = 0.15$ are shown in Figure 3-6. A shift of energy from the higher to the lower frequencies is observed in a frequency range from approximately $40Hz$ to $150Hz$. This observation is consistent with linear stability theory which predicts the selective amplification of increasingly lower frequencies as the distance downstream of the leading edge increases.

Spanwise spectra at $x = 1.00m$, $U/U_o = 0.15$ are shown in Figure 3-7. These

measurements were taken $4.5cm$ apart, $13.5cm$ on each side of the centerline. The results show consistent spectra with some variation at frequencies near $50Hz$ resulting from the positive spanwise locations. This is most likely due to a redistribution of traverse vibration energy when the instrumentation platform is low on the z-traverse, shifting the center of mass of the traverse and raising the natural frequency. The peak observed near $520Hz$ appears in all measurements and has not been explained.

3.3 Summary

- Characterization of the mean flow over a smooth plate indicates a slightly favorable pressure gradient which corresponds to a Falkner-Skan solution of $\beta = 0.0155$. This solution was used as the smooth plate baseline flow in the remaining studies.

- Streamwise deviation of the mean flow from Falkner-Skan varied from one to three percent between $R_{\delta^*} = 1080$ and $R_{\delta^*} = 1450$. Average spanwise variations were within five percent of the Falkner-Skan solution.

- The smooth plate freestream velocity spectrum reveals a low disturbance environment with a resulting freestream turbulence level less than 0.08% of the mean velocity at $12.5 m/s$.

- Facility noise components which were found to amplify in the boundary layer spectra were identified and determined not to have a significant effect on roughness experiment results.

Chapter 4

Two-Dimensional Roughness Arrays

The results and discussion presented in this chapter deal with two-dimensional, three-element roughness arrays and their role in boundary layer receptivity and transition. Limited investigation of the effects of single-element and five-element arrays was performed to assist in analyzing three-element array results.

4.1 Theoretical Small Disturbance Amplification

Amplification curves based on linear stability theory were computed for the Falkner-Skan solution ($\beta = 0.0155$) which corresponds to the mean flow results discussed earlier. These curves are shown in Figure 4-1 where Reynolds number is based on displacement thickness, F is the nondimensional frequency of the disturbance defined by $F \times 10^{-6} = (2\pi f\nu)/U_o^2$, f is the dimensional frequency, and ν is the kinematic viscosity. Values for $50 \leq F \leq 120$ (increments of 10) are shown with increasing F to the left of the figure. The frequency of interest in this study, $F = 70$ or $f = 115Hz$, is represented with a dashed line.

These curves represent the growth and decay of small disturbances or velocity fluctuations in the boundary layer. Selected frequencies associated with the fluctuations begin to amplify at branch I, the concave portion of each curve, and continue

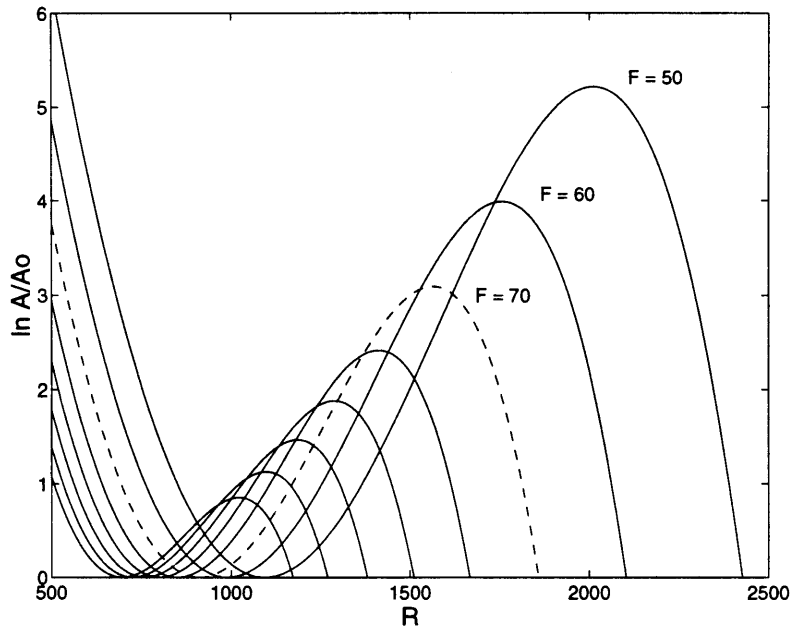

Figure 4-1: Amplification curves for Falkner-Skan $\beta = 0.0155$. Values for $F = 50$ to $F = 120$ (increments of 10) are shown with F increasing to the left of the figure. $F = 70$ is represented with a dashed line as the frequency of interest.

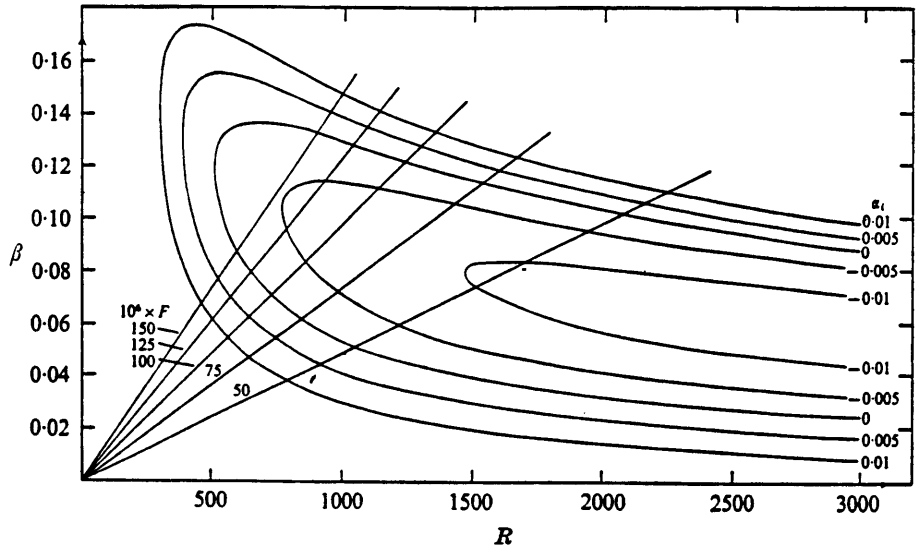

Figure 4-2: Stability curves of constant α_i for a flat plate, $\beta = FR$. Reproduced from Jordinson [7].

to amplify to branch II, the convex portion of each curve, as the Reynolds number increases. Beyond branch II, the disturbances again begin to decay.

Another way of graphically displaying the growth and decay of disturbances is shown in Figure 4-2 taken from Jordinson [7]. Beta, which is plotted on the y-axis, is not the Beta associated with the Falkner-Skan solution but rather a nondimensional representation of the angular frequency ω where $\beta = FR$. One can select a line of constant frequency and determine the range of Reynolds numbers over which the disturbance is amplifying or decaying. Positive values of the imaginary component of the wave number, α_i, indicate decaying fluctuations while negative values indicate amplification with $\alpha_i = 0$ representing neutral stability.

4.2 Roughness Array Structure and Receptivity

The figures representing the stability of disturbances in the boundary layer also provide a basis for selecting the roughness array location for these investigations. An unforced frequency of $f \simeq 115Hz$ ($F = 70$) was selected as the frequency of interest in which growth and decay are monitored as a function of various roughness parameters for each experiment. Branch I, indicating the start of amplification of this frequency, is located at $R_{\delta^*} = 930$ ($x = 0.37m$) at $12.5m/s$ as shown in Figure 4-1. Wiegel and Wlezien [13] performed similar experiments in which they selected $80Hz$ as the frequency of interest, locating their roughness array at the corresponding branch I location. Choosing the center of the roughness array to correspond with branch I provides the disturbances with large initial amplitude and greater amplification as they move downstream [12].

Spacing of a three-element array at branch I with $k = 0.24mm$ was investigated to determine the distance which would provide greatest amplification of the selected frequency downstream of the roughness. The intent was to provide a mechanism for maximizing receptivity in the boundary layer by providing the appropriate conditions for external disturbance wavelength scattering. This was done by matching the appropriate short scale wavelength of the selected frequency with the roughness

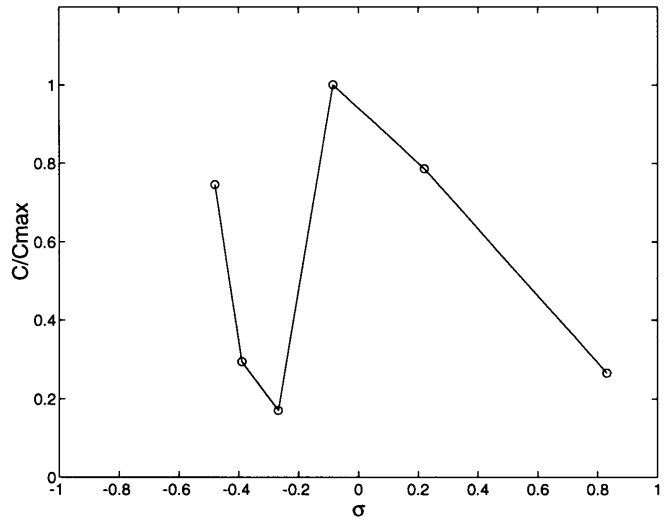

Figure 4-3: Receptivity coefficient versus detuning parameter for $f = 115Hz$ at $R_{\delta^*} = 1603$, $U_o = 12.5m/s$, $U/U_o = 0.30$.

structure spacing and varying the wavelength slightly to observe a detuning effect. Results are presented in Figure 4-3 using the method of Wiegel and Wlezien [13].

The x-axis in this figure represents the detuning effect defined by $\sigma = (\lambda_{ts} - \lambda_w)/\lambda_w$ where $\lambda_{ts} = 3.66cm$ is the T-S wavelength at branch I and λ_w is the spacing between roughness elements in the array. The T-S wavelength was determined from $\lambda = (2\pi\delta^*)/\alpha_r$. The receptivity coefficient is defined by $\hat{u}_{ts}/\hat{u}_{ac}$ where $\hat{u}_{ts}$ is the amplitude of the T-S wave at branch I and $\hat{u}_{ac} = 0.01m/s$ is the amplitude of the external disturbances.

The resulting optimal spacing, based on the distances measured in this experiment, corresponded approximately to the selected frequency wavelength at branch I of the stability curve. This can be observed from Figure 4-3 where receptivity increases as the roughness spacing approaches the selected frequency wavelength. A peak in receptivity occurs near a detuning parameter equal to zero which corresponds to roughness spacing at the wavelength of the selected frequency. As the roughness spacing continues to increase, the detuning parameter decreases along with receptivity. Although a direct comparison is difficult to make, these results are in qualitative

$x_k[m]$	$k[mm]$	$\delta_k^*[mm]$	k/δ_k^*	$R_{\delta_k^*}$
0.370	0.12	1.12	0.107	930
0.370	0.24	1.12	0.214	930
0.370	0.36	1.12	0.321	930

Table 4.1: Three-element roughness array parameters.

agreement with observations of Wiegel and Wlezien [13] who varied the freestream velocity rather than roughness spacing to observe the detuning effect. Spacing was increased further in this experiment to show a trend toward another peak in receptivity as the spacing approached twice the selected frequency wavelength.

The final roughness configuration consisted of three rows of roughness spaced $4cm$ apart with the array spanning $R_{\delta^*} = 878$ to 979, centered at $R_{\delta^*} = 930$. Three different roughness heights, k, were examined to give $k/\delta_k^* = 0.107$, 0.214, and 0.321. The value for δ_k^* was determined using the streamwise location of the center element of the array. The relevant roughness parameters are shown in Table 4.1 where x_k is the roughness location, k is the roughness height, δ_k^* is the displacement thickness at the roughness location in the absence of roughness, and $R_{\delta_k^*} = 1.68\sqrt{\frac{U_o\delta_k^*}{\nu}}$ is the roughness Reynolds number.

4.3 Results and Discussion

4.3.1 Velocity Spectra

Velocity spectra were measured every $0.20m$ downstream of the roughness array for $k/\delta_k^* = 0.107$ and 0.214 beginning at $R_{\delta^*} = 1080$ ($x = 0.50m$) until transition was observed. For $k/\delta_k^* = 0.321$, measurements were taken every $0.10m$ to provide better resolution before transition. Spectral measurements were taken at $U/U_o = 0.15$, where $U_o = 12.5m/s$. Resulting spectra for $k/\delta_k^* = 0.107$, 0.214, and 0.321 are shown in Figures 4-4, 4-5, and 4-6 respectively.

Looking first at the spectra for $k/\delta_k^* = 0.107$ in Figure 4-4, several observations can be made. Between $R_{\delta^*} = 1080$ and 1450 there is no observable deviation from the

smooth plate spectra shown in Figure 3-6 except at $f \simeq 115Hz$ where slight amplification is occurring. At $R_{\delta^*} = 1603$ increased amplification of disturbance frequencies near $f \simeq 115Hz$ results in marked deviation from the smooth plate measurements. Since the amplitude of the fluctuations corresponds to a square root change in power density, an amplification approximately 6 times that of the smooth plate is observed at this location. This Reynolds number corresponds to branch II on the stability curve for $f = 115Hz$ which is where this frequency would be most amplified.

As Reynolds number continues to increase, the amplified frequency does not begin to decay as predicted from linear stability theory for a smooth plate. By $R_{\delta^*} = 1872$ all frequencies have become significantly amplified and the boundary layer begins to transition.

Progression of the velocity spectra for this low-level roughness configuration reflects an increase in receptivity. Transition occurs 9 percent earlier in R_{δ^*}, calculated as a deviation from the smooth plate transition location of $R_{\delta^*} = 2051$, and a transfer of energy to the selected frequency is apparent. These observations are in qualitative agreement with previous work.

Spectra for $k/\delta_k^* = 0.214$, Figure 4-5, reveal a greater effect of roughness on stability of the boundary layer. At $R_{\delta^*} = 1080$, a small band of amplified high frequencies appears near $f \simeq 200Hz$ which did not appear in the smooth plate or $k/\delta_k^* = 0.107$ spectra. This band corresponds to the modes which would be amplified near $R_{\delta^*} = 1080$ as predicted by linear stability theory but which might not have been noticeable due to the short amplification period. In the presence of roughness elements with sufficient amplitude to energize these high frequencies, they become noticeable in the velocity spectra before beginning to decay.

An increase in Reynolds number causes a shift of disturbance energy from the high frequencies to the lower frequencies. At $R_{\delta^*} = 1278$, a well-defined peak in the power density appears near $f = 165Hz$ which corresponds to the branch II location of this frequency on the stability curve. This energy continues to redistribute to the lower frequencies where at $R_{\delta^*} = 1450$ amplification at the selected frequency is clearly visible. The increased rate in amplification of $f = 115Hz$ distinguishes the effect of

this roughness height from the previous results. At $R_{\delta^*} = 1603$, the amplitude of $f = 115Hz$ has increased to a factor of 10 over that of the smooth plate. Transition occurs beyond this location approximately 22 percent further upstream in Reynolds number than for the smooth plate case.

A well defined higher harmonic centered at $230Hz$ is also established by $R_{\delta^*} = 1603$. Increased receptivity generates instabilities at this selected frequency making it a dominant mode. Since all frequencies are of comparable amplitude, nonlinear resonant interactions can occur between modes. This interaction continues to occur even if the dominant mode is linearly damped (for a complete discussion of resonant nonlinear behavior see [5]). These resonant nonlinear interactions were not noted in the work of Wiegel and Wlezien [13].

The most significant effect of the roughness array on instability amplification can be seen in Figure 4-6 for $k/\delta_k^* = 0.321$. At $R_{\delta^*} = 1080$, a large band of high frequencies centered near $f = 200Hz$ have been amplified by a factor of 10 over that of the smooth plate. Again, an increase in roughness height shows a significant increase in amplification of the higher frequencies which would not have had the energy to show significant amplitude before decaying. As witnessed in the smaller amplitude arrays, the high frequency energy redistributes to the lower frequencies with increasing Reynolds number.

Amplification of the selected frequency is apparent immediately downstream of the roughness array and continues until transition occurs just beyond $R_{\delta^*} = 1450$. The transition location is 30 percent further upstream in Reynolds number than for the smooth plate. Amplitude of the selected frequency prior to transition is approximately 18 times larger than the smooth plate amplitude.

In this configuration, a second, third, and even fourth harmonic can be seen. As described previously, higher modes begin to interact nonlinearly with the fundamental frequency to produce additional harmonics and to influence existing modes. An interesting observation is the matching peak to peak of the harmonics. For example, the fan blade passage frequency is distinctly visible as a sharp peak in all harmonics.

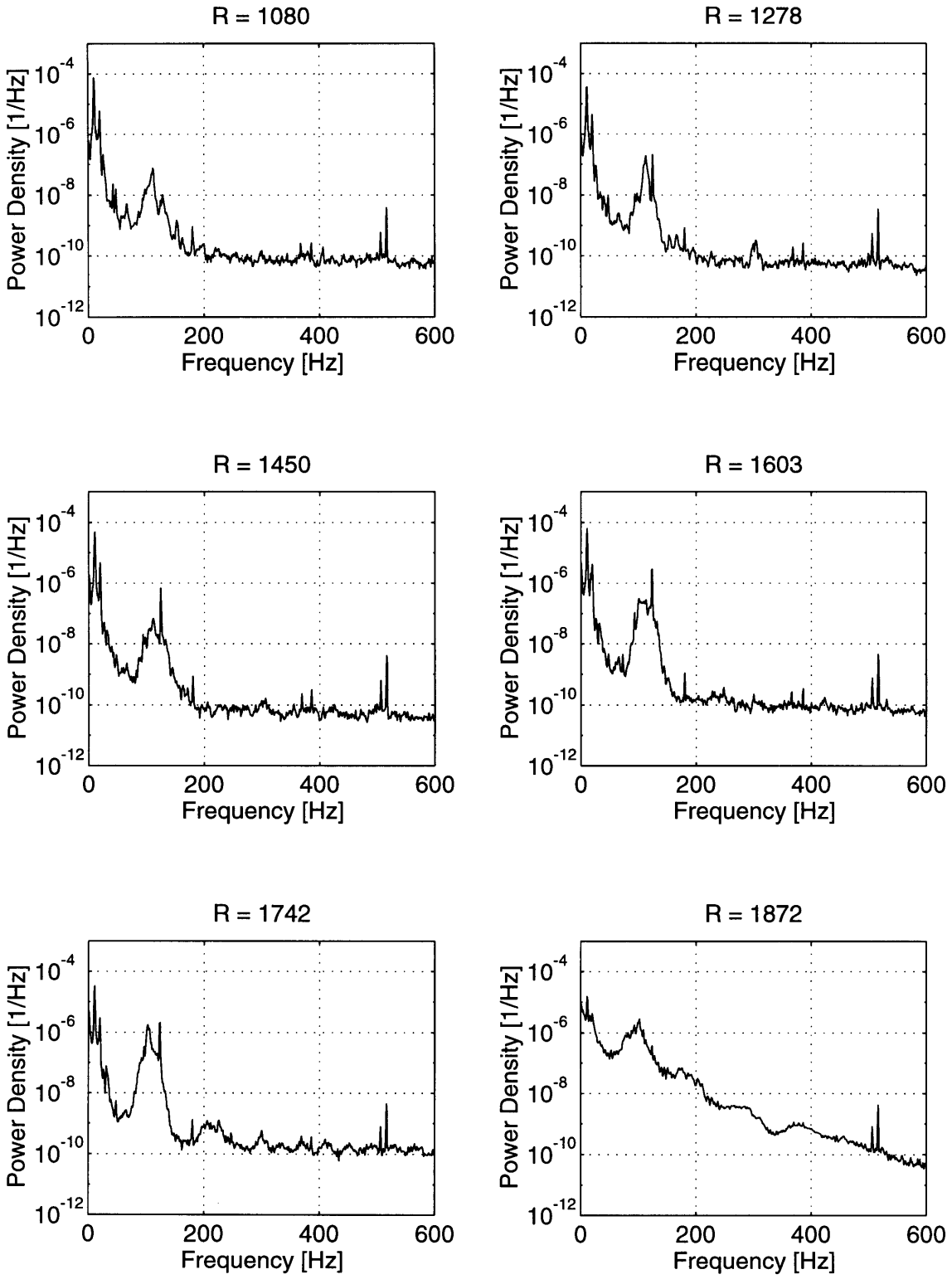

Figure 4-4: Spectral evolution for $k/\delta_k^* = 0.107$, three-element array, $U/U_o = 0.15$, $U_o = 12.5m/s$. Reynolds number based on displacement thickness. Power density normalized by U_o^2.

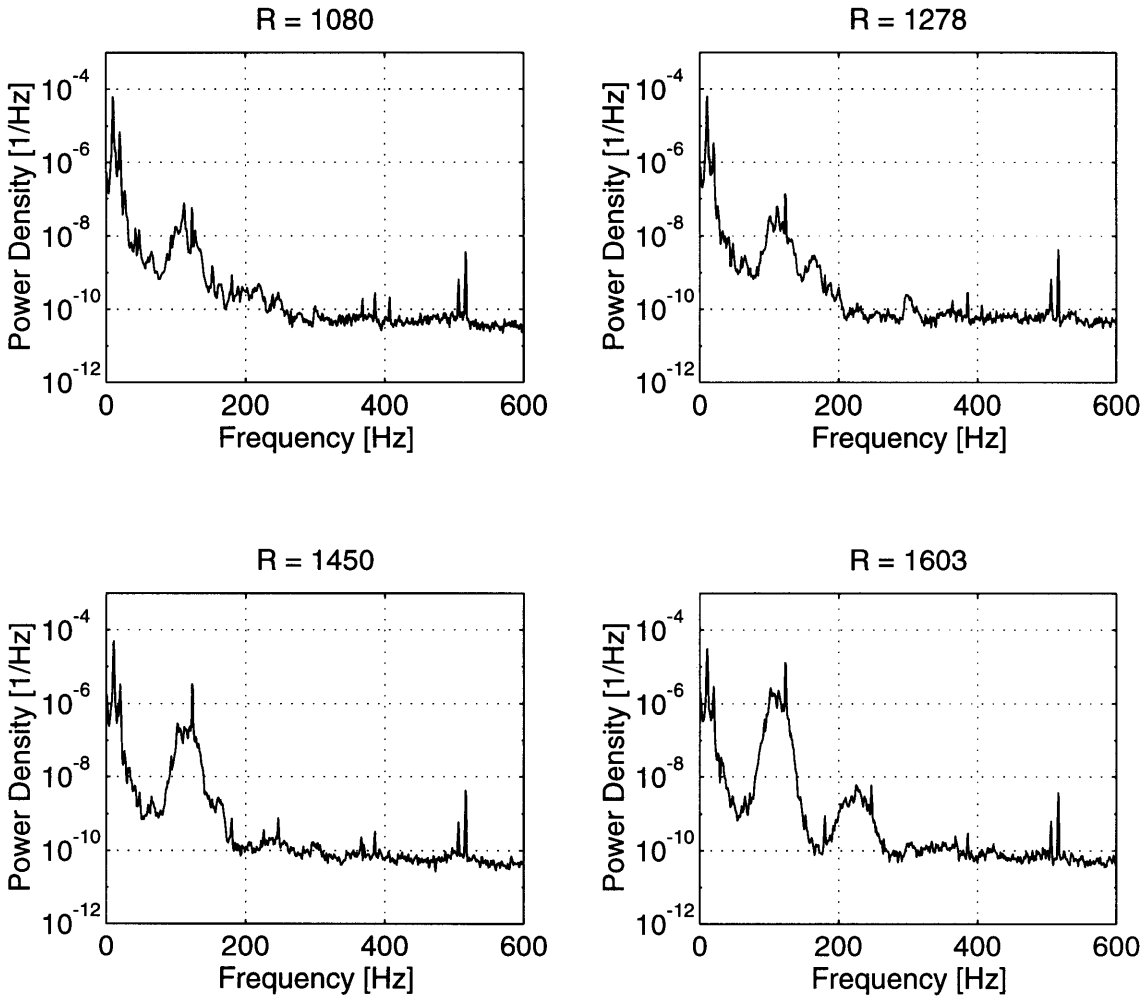

Figure 4-5: Spectral evolution for $k/\delta_k^* = 0.214$, three-element array, $U/U_o = 0.15$, $U_o = 12.5m/s$. Reynolds number based on displacement thickness. Power density normalized by U_o^2.

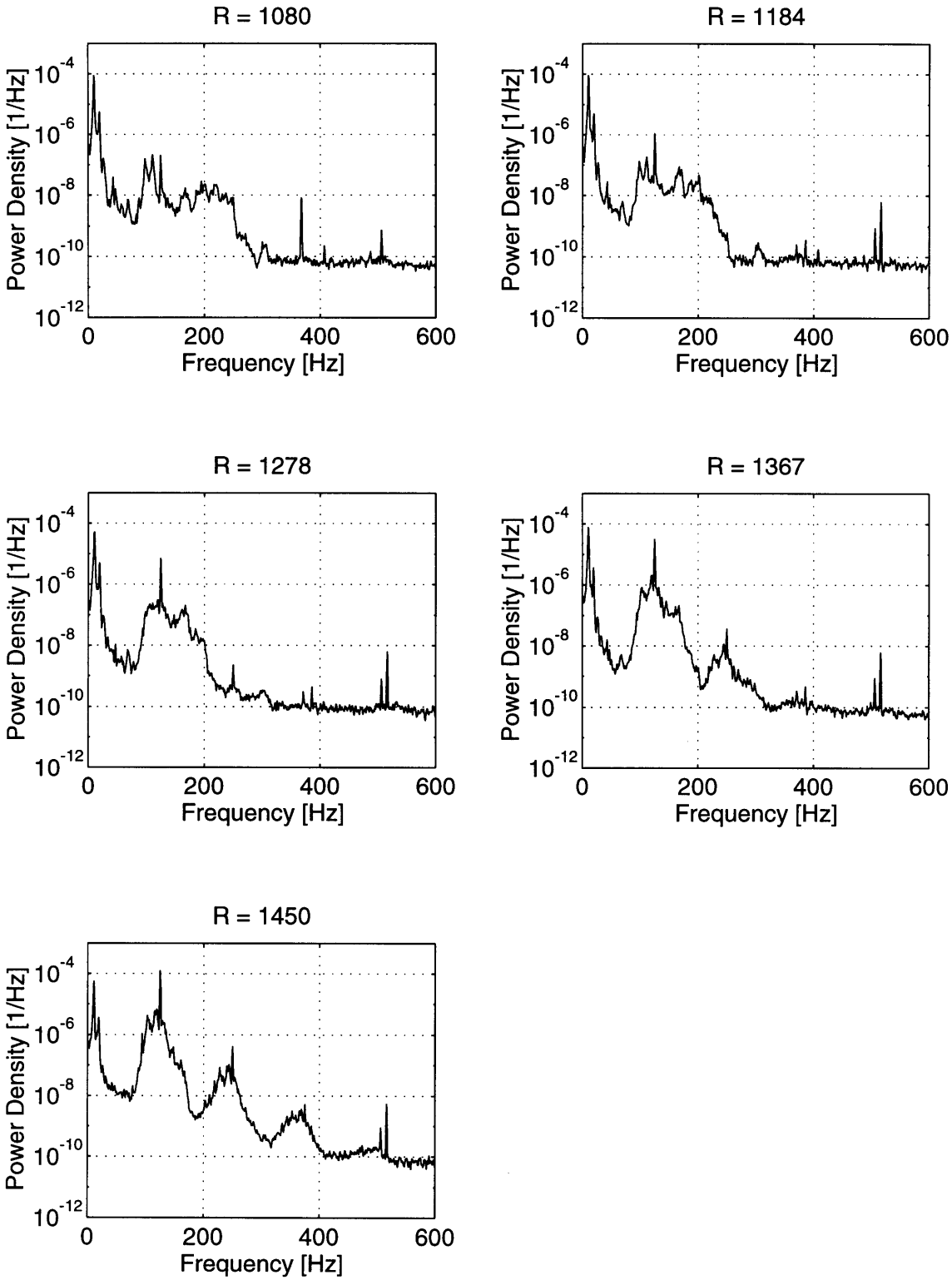

Figure 4-6: Spectral evolution for $k/\delta_k^* = 0.321$, three-element array, $U/U_o = 0.15$, $U_o = 12.5m/s$. Reynolds number based on displacement thickness. Power density normalized by U_o^2.

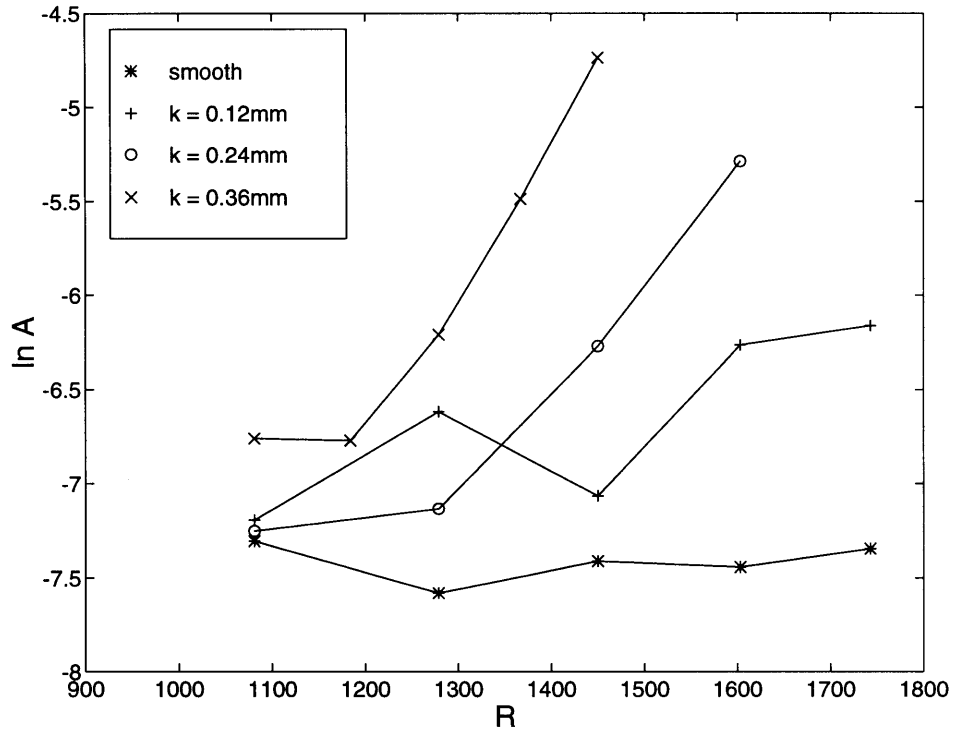

Figure 4-7: Amplification of the frequency band $110Hz \leq f \leq 120Hz$ for a three-element array of varying amplitude with increasing R_{δ^*}. $U/U_o = 0.15$, $U_o = 12.5m/s$. Amplitude normalized by U_o.

4.3.2 Amplification of the Selected Frequency

The effect of roughness height on amplification of the selected frequency, $f = 115Hz$, is shown in Figure 4-7. Comparable growth rates between the different roughness heights can be seen with the possibility of a slightly higher amplification rate displayed by $k/\delta_k^* = 0.321$. Smooth plate results do not show amplification immediately downstream of branch I ($R_{\delta^*} = 930$) as predicted by linear stability theory. This may be explained by the unforced disturbance level which is allowing linear as well as nonlinear interactions to occur between disturbances generated by background noise.

Resolution in the number of measurements makes it difficult to determine the trend in amplification beyond branch II which is located at $R_{\delta^*} = 1560$. Theory predicts the decay of the selected frequency beyond this point, however this is only

observed in the results for $k/\delta_k^* = 0.107$ and is not obvious at the other roughness amplitudes.

The data point for $k/\delta_k^* = 0.107$ at $R_{\delta^*} = 1278$ deviates significantly from the observed trend in disturbance amplification. This value was derived from the velocity spectrum shown in Figure 4-4. A sharp peak can be seen in this figure near $f = 115Hz$ which is believed to have resulted from a disturbance in the facility at the time of the measurement.

The largest roughness height shows the greatest rate of amplification at the selected frequency. The rate of amplification is seen to increase with an increase in roughness height. Since the energy imparted to the disturbance at branch I is greatest for the largest roughness height, one would expect the largest disturbance amplitude prior to transition to correspond with this same roughness height.

4.3.3 Fourier Analysis and Amplitude Scaling

To quantify the relative effect of the different roughness heights and number of elements in the array, a Fourier transform of the roughness array can be performed [2]. Equation 4.1 gives the Fourier transform for a single roughness element of width L and height k where α is the wavenumber. A linear relation exists between the forcing function $F(\alpha)$ of the roughness and the fluctuation amplitude due to the roughness.

$$F(\alpha) = \int_{-L/2}^{L/2} f(x) e^{i\alpha x} dx \tag{4.1}$$

$$f(x) = \begin{cases} k & \frac{-L}{2} \leq x \leq \frac{L}{2} \\ 0 & \text{otherwise} \end{cases}$$

The resulting Fourier kernel for one roughness element can be seen to scale linearly with the height k of the roughness element in Equation 4.2.

$$F(\alpha) = \frac{2k}{\alpha} sin \frac{\alpha L}{2} \tag{4.2}$$

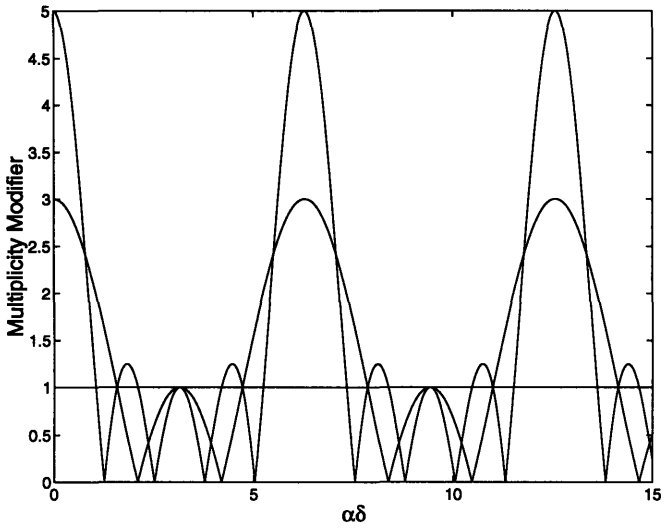

Figure 4-8: Forcing function of the Fourier transform for 1, 3, and 5 elements in the roughness array.

This kernel is modified based on the number of elements in the array, N, spaced a distance δ apart. The resulting transforms containing the modifiers are shown below for roughness arrays containing 1, 3, and 5 elements.

$$F(\alpha) = \begin{cases} \frac{2k}{\alpha} sin\frac{\alpha L}{2} & N = 1 \\ \frac{2k}{\alpha} sin\frac{\alpha L}{2}[1 + 2cos\,\alpha\delta] & N = 3 \\ \frac{2k}{\alpha} sin\frac{\alpha L}{2}[1 + 2cos\,\alpha\delta + 2cos\ 2\alpha\delta] & N = 5 \end{cases}$$

A plot of the absolute value of the modifier is shown in Figure 4-8. From this figure it can be seen that the maximum value of $F(\alpha)$ exists at $\alpha\delta = 2\pi$ and that the forcing due to the modifier scales linearly. These Fourier transform results can be used to verify the different experimental results for various roughness configurations.

Figure 4-9 shows the effect of linearly scaling the amplitude of the fluctuations based on a difference in roughness height at $R_{\delta^*} = 1603$. The spectra for $k/\delta_k^* = 0.107$ and $k/\delta_k^* = 0.214$ are shown unscaled on the left side of the figure with the lower power density curve representing $k/\delta_k^* = 0.107$. The right side of the figure shows the power density for $k/\delta_k^* = 0.107$ scaled by a factor of $(2)^2$ to match the power

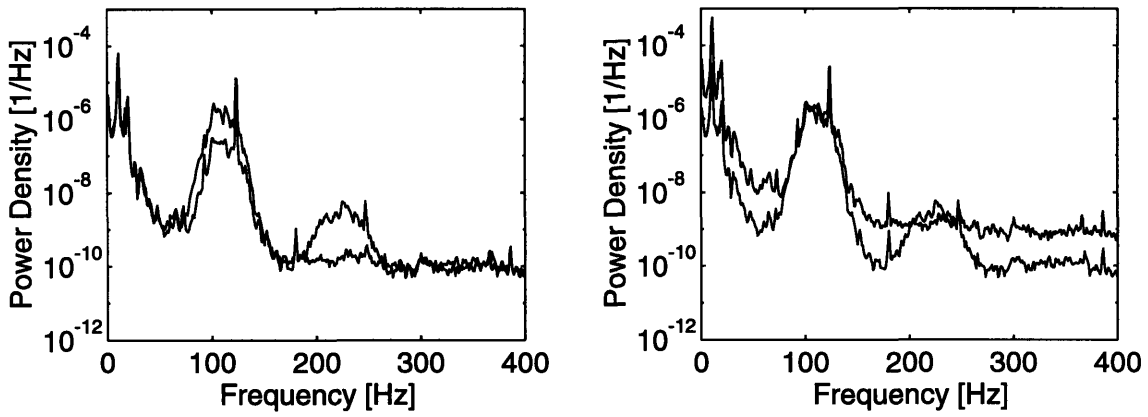

Figure 4-9: Scaling of $k/\delta_k^* = 0.107$ to $k/\delta_k^* = 0.214$ for a three-element array at $R_{\delta^*} = 1603$, $U/U_o = 0.15$, $U_o = 12.5m/s$. Power density normalized by U_o^2.

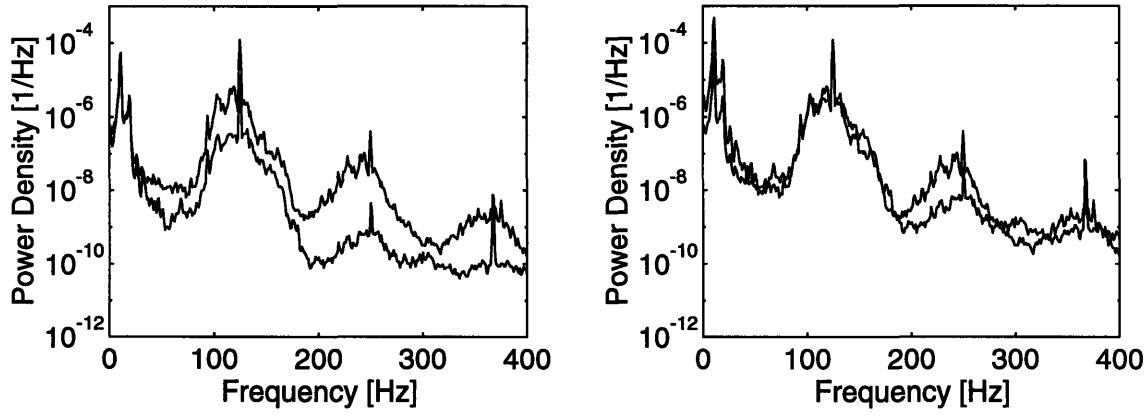

Figure 4-10: Scaling of $k/\delta_k^* = 0.321$ for a single-element array to $k/\delta_k^* = 0.321$ for a three-element array at $R_{\delta^*} = 1450$, $U/U_o = 0.15$, $U_o = 12.5m/s$. Power density normalized by U_o^2.

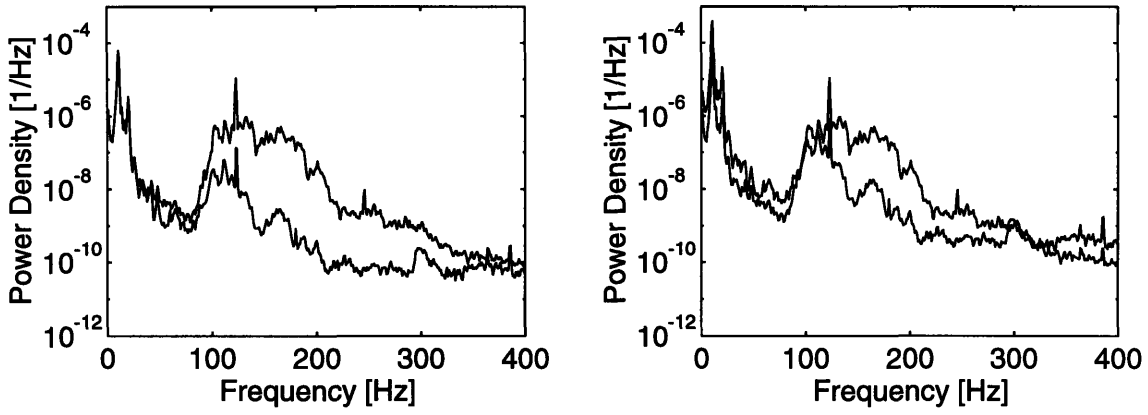

Figure 4-11: Scaling of $k/\delta_k^* = 0.214$ for a three-element array to $k/\delta_k^* = 0.321$ for a five-element array at $R_{\delta^*} = 1278$, $U/U_o = 0.15$, $U_o = 12.5m/s$. Power density normalized by U_o^2.

density of $k/\delta_k^* = 0.214$. Referring to Equation 4.2, the scaling factor is based on the square of the difference in amplitude of the roughness which determines the difference in power density. This result shows good agreement between experiment and theory.

Figure 4-10 shows the result of linear scaling based on the different number of elements in the array. The spectra for $k/\delta_k^* = 0.321$ for an array of one versus an array of three at $R_{\delta^*} = 1450$ is shown unscaled in the plot on the left. The lower power density curve corresponds to the single-element array which is scaled by a factor of $(3)^2$ to match the power density of the three-element array as shown in the plot on the right.

Both examples discussed so far have shown the apparent linear scaling of fluctuation amplitudes for roughness heights up to $k = 0.36mm$ and $k/\delta_k^* = 0.321$. This is in agreement with observations of Saric *et al.* [11] who demonstrated a linear relationship between roughness height and receptivity for $0.04mm \leq k \leq 0.12mm$ at $k/\delta_k^* = .030$ using acoustic forcing. Beyond $k = 0.20mm$ for $k/\delta_k^* = 0.134$ and 0.168, Saric observed nonlinearity which may have resulted from the high level of acoustic forcing.

Figure 4-11 shows the result of linear scaling based on both the number of elements in the array and the roughness height. The spectrum for $k/\delta_k^* = 0.214$ for an array of

three and the spectrum for $k/\delta_k^* = 0.321$ for an array of five at $R_{\delta^*} = 1278$ are shown unscaled in the plot on the left. The power density for the smaller array is scaled by a factor of $(3/2)^2(5/3)^2$ to match the power density of the five element array in the plot on the right. Linear scaling does not work as well in this case as it did in the previous results. Although the selected frequency appears to scale well, the five element roughness array for $k/\delta_k^* = 0.321$ generates a band of high frequencies which are not as evident in the weaker forcing results and which do not scale linearly.

Another interesting amplitude scaling comparison can be performed on the harmonics. Figure 4-12a shows the unscaled spectra of $k/\delta_k^* = 0.321$ for a single-element array and a three-element array at $R_{\delta^*} = 1450$. The scaling factor applied to the single-element results at the fundamental frequency in Figure 4-12b is $(3)^2$ based on the difference in the number of elements in the array. In Figure 4-12c where the second harmonic is scaled, a factor of $((3)^2)^2$ was necessary to account for the quadratic scaling of the higher harmonic.

The growth of a subharmonic mode would be expected due to the resonant nonlinear interactions which are occurring. For example, in wave packets in the boundary layer, the subharmonic mode was observed to be a dominant resonant nonlinear interaction [4]. In the present experiments at $U/U_o = 0.15$, a subharmonic is detected in the spectra for $k/\delta_k^* = 0.321$ where strong harmonics are also observed. This can be seen in Figure 4-6 at $R_{\delta^*} = 1450$ where a band of frequencies centered near $50Hz$ is amplified with the appearance of a third and fourth harmonic. A subharmonic was not apparent for $k/\delta_k^* = 0.107$ and 0.214, or in the single-element experiments at $U/U_o = 0.15$. However, at $U/U_o = 0.30$, a clear subharmonic peak was observed for all roughness arrays prior to the onset of transition. For $k/\delta_k^* = 0.107$ and 0.214 the subharmonic approached a comparable amplitude to the fundamental mode. Further investigation of the subharmonic mode is recommended based on these observations, but was not pursued in this research.

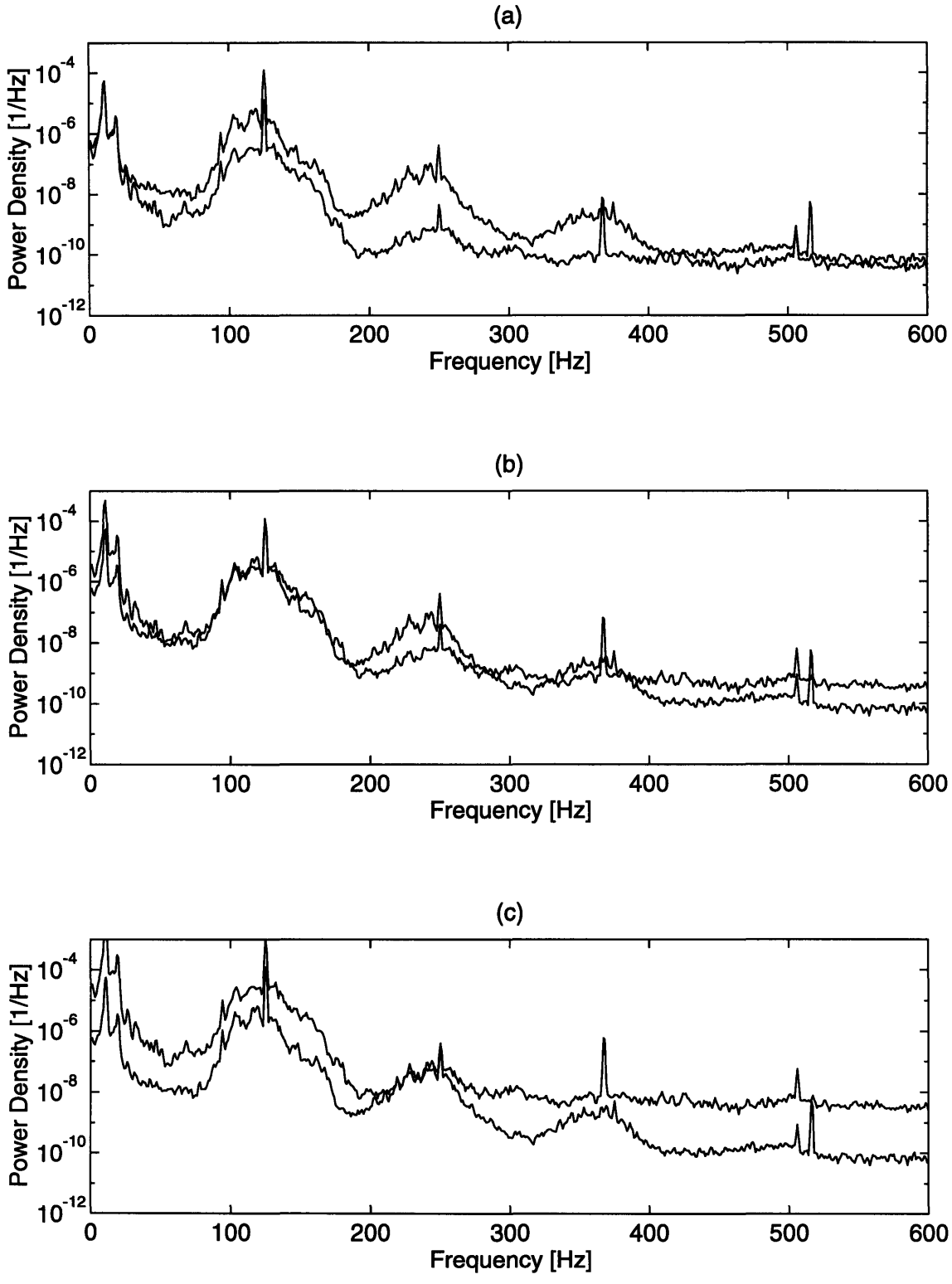

Figure 4-12: Scaling of harmonics for $k/\delta_k^* = 0.321$ for a three-element and single-element array at $R_{\delta^*} = 1450$, $U/Uo = 0.15$, $U_o = 12.5m/s$. Power density normalized by U_o^2.

4.3.4 Mean Flow Profiles

Velocity profiles were measured for all three roughness array amplitudes at $R_{\delta^*} =$ 1080, 1278, and 1450 ($x = 0.50m$, $0.70m$, and $0.90m$). Deviations from the Falkner-Skan profile are shown in Figure 4-13 along with the smooth plate curve fit deviation indicated by the solid line. Results indicate that the roughness elements have an increasing effect on mean flow distortion as the distance downstream of the roughness increases. This is most likely due to the increased nonlinear effects of the roughness-induced velocity fluctuations.

At $R_{\delta^*} = 1080$, a trend in mean flow deviation close to that of the smooth plate is observed for all roughness amplitudes with results for $k/\delta_k^* = 0.321$ appearing to deviate slightly more than the others. Further downstream at $R_{\delta^*} = 1278$, a varied effect of roughness amplitude on the mean flow is observed. Deviation from Falkner-Skan due to the smallest amplitude array remains comparable to the smooth plate while the results for $k/\delta_k^* = 0.214$ and 0.321 show an increasing distortion of the mean flow. The final location which was measured at $R_{\delta^*} = 1450$ produces inconclusive results in deviation trends for the various roughness amplitudes. It is difficult to identify whether or not the flow is relaxing to the undisturbed profile or continuing to diverge since the onset of transition is beginning to influence the flow.

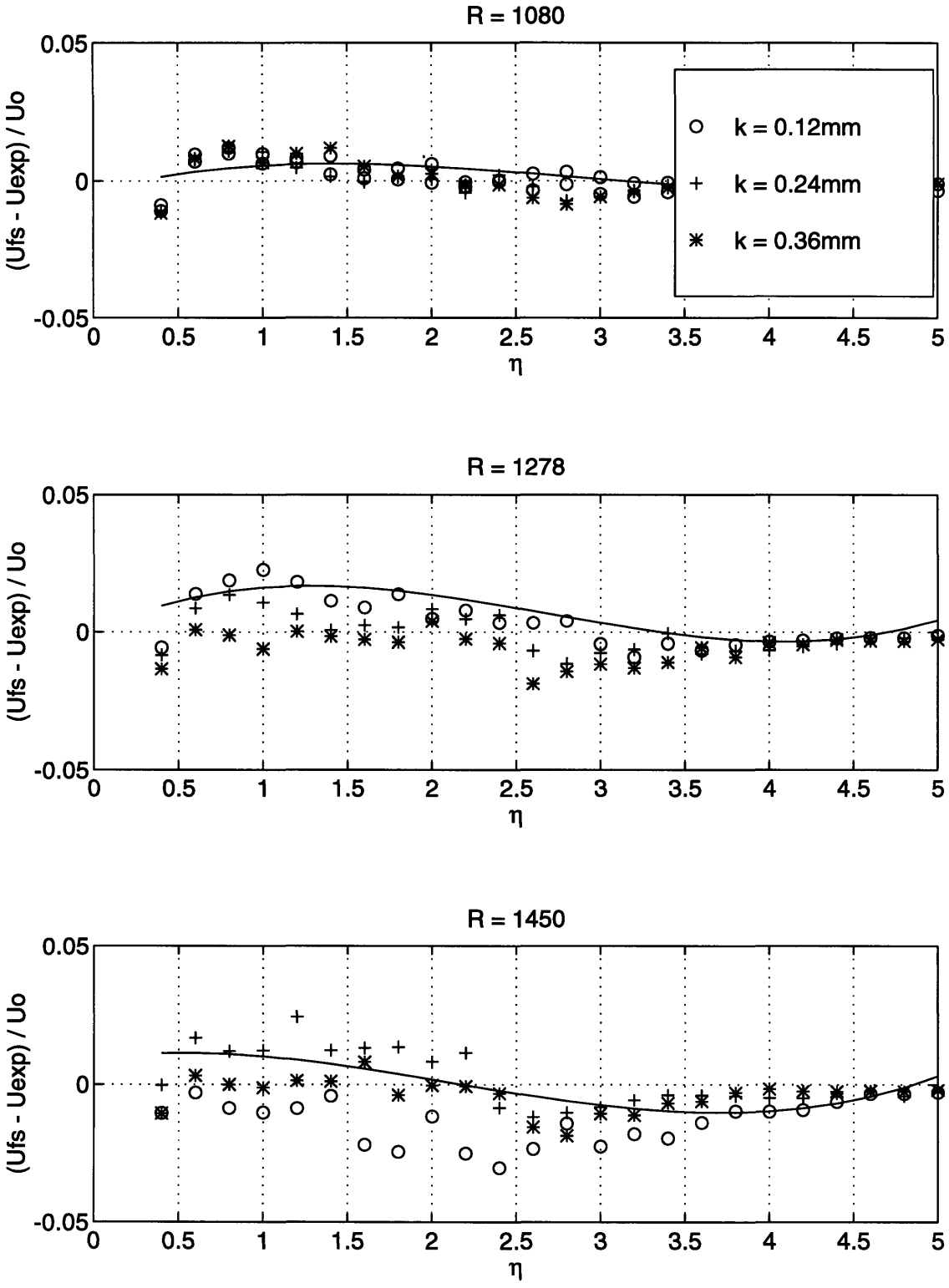

Figure 4-13: Experimental mean flow deviation from Falkner-Skan $\beta = 0.0155$, $U_o = 12.5m/s$. Measurements made at centerline locations for $R_{\delta^*} = 1080$, 1278, and 1450 ($x = 0.50m$, $0.70m$, and $0.90m$). Solid line represents a third order polynomial curve fit for the smooth plate results.

4.4 Summary

- Three-element roughness arrays of amplitude $k = 0.12mm$, $0.24mm$, and $0.36mm$ were shown to have an effect on boundary layer receptivity. Array spacing, chosen to match the T-S wavelength of a selected frequency, and roughness placement at the corresponding branch I of the stability curve provided the mechanism for maximizing these results.

- An increased effect on transition with increased roughness height was observed. Transition occurred roughly 9, 22, and 30 percent earlier in Reynolds number, R_{δ^*}, for $k/\delta_k^* = 0.107$, 0.214, and 0.321 respectively.

- Nonlinear resonant interactions between the selected mode and higher harmonics were observed. Larger amplitude roughness produces more harmonics and also shows a higher rate of amplification of the selected frequency.

- Perturbation amplitudes scaled linearly with roughness height and the number of elements in the array. Higher harmonics were shown to scale quadratically.

- A subharmonic mode was found to exist for all levels of roughness at a boundary layer location of $U/U_o = 0.30$. Further investigations at this location are recommended.

- Deviation of the experimental mean flow results from the Falkner-Skan solution were determined for all roughness amplitudes. Immediately downstream of the roughness the deviation is comparable to the smooth plate result. However, as the distance downstream increases, mean flow distortion increases for the larger amplitudes of roughness most likely due to increased nonlinear effects of the velocity fluctuations. Prior to transition it is difficult to observe any significant trends in deviation.

Chapter 5

Two-Dimensional Single-Element Roughness

In moving from studies of multi-element roughness arrays to single-element roughness of greater amplitude, the role of two-dimensional roughness in boundary layer transition has shifted. Receptivity, and therefore the effect of multiple elements in the roughness array, is less of an issue as an increase in roughness height allows nonlinear, mean flow distortion mechanisms to dominate.

Results for $k/\delta_k^* = 0.321$ in the previous experiments showed a trend toward amplification of higher frequencies. However, the roughness amplitude was still small enough to allow linear mechanisms to dominate and follow the path to transition predicted by linear theory. As the roughness parameter is increased to $k/\delta_k^* = 0.64$ in the following experiments, broad-band, high frequency amplification and the deviation from linear mechanism results are of primary interest.

5.1 Roughness Parameters

Boundary layer transition was investigated for three different roughness Reynolds numbers, $R_{\delta_k^*}$. The parameter k/δ_k^* was held constant by moving the roughness location downstream as k was increased and U_o was held constant. Relevant roughness parameters are shown in Table 5.1.

$x_k[m]$	$k[mm]$	$\delta_k^*[mm]$	k/δ_k^*	$R_{\delta_k^*}$
0.370	0.72	1.12	0.64	927
0.657	0.96	1.50	0.64	1242
1.027	1.20	1.87	0.64	1549

Table 5.1: Single-element roughness parameters.

5.2 Results and Discussion

5.2.1 Mean Flow Profiles

Velocity profiles were measured downstream of the roughness elements with constant $k/\delta_k^* = 0.64$ to examine the effect of large amplitude roughness on mean flow distortion. Results for $R_{\delta_k^*} = 927$, 1242, and 1549 are shown in Figures 5-1, 5-2, and 5-3 respectively.

Profiles for $R_{\delta_k^*} = 927$ and 1242 were adjusted in η based on a least squares fit of the near wall measurements. A qualitative assessment of mean flow distortion based on these profiles is difficult because a slight error in adjustment of η can result in an over-developed or under-developed flow. As presented in Figures 5-1 and 5-2 with the linear extrapolation method, the results show a flow which is accelerating over the roughness element and relaxing to the smooth plate solution downstream of the roughness. This is in agreement with observations of Klebanoff and Tidstrom [9] for $k/\delta_k^* = 0.72$, 0.77, and 0.86, however, they also observed an initially inflected profile due to separation. Although separation is not apparent in the present results, it is possible that it is occurring and by $x - x_k = 4mm$, the flow has already begun to recover as viscous forces act to drive the mean flow back towards a self-similar solution. It also appears from the present results that the flow is over-relaxed before returning to the smooth plate solution. This was not observed by Klebanoff and Tidstrom and may be the result of an error in shifting the profile.

Results for $R_{\delta_k^*} = 1549$ shown in Figure 5-3 clearly demonstrate the effect of separation in distorting the mean flow. These profiles were shifted in η to match the Falkner-Skan solution near the freestream. Since separation was strongly evident, the

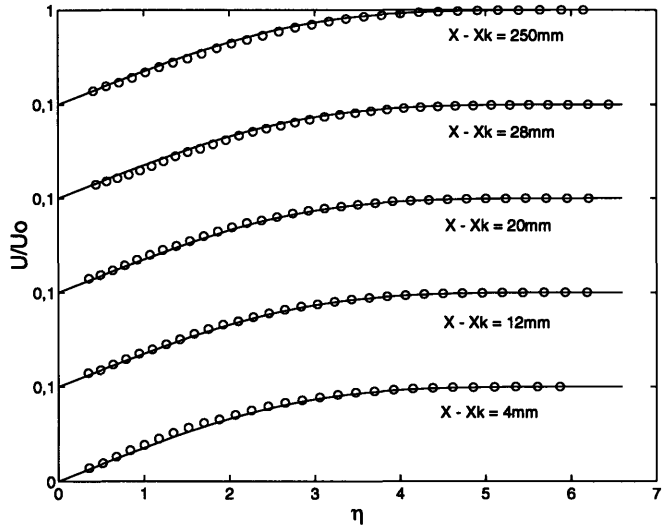

Figure 5-1: Experimental mean flow data for $R_{\delta_k^*} = 927$ (o) and Falkner-Skan $\beta = 0.0155$ (-), $U_o = 12.5m/s$, $R_{\delta^*} = 935$, 945, 955, 964, and 1204. Edge of roughness located at $\eta = 1.075$.

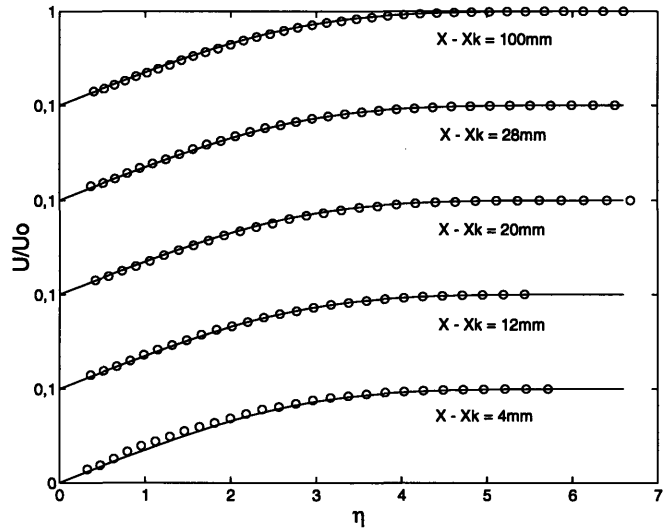

Figure 5-2: Experimental mean flow data for $R_{\delta_k^*} = 1242$ (o) and Falkner-Skan $\beta = 0.0155$ (-), $U_o = 12.5m/s$, $R_{\delta^*} = 1243$, 1250, 1258, 1265, and 1330. Edge of roughness located at $\eta = 1.075$.

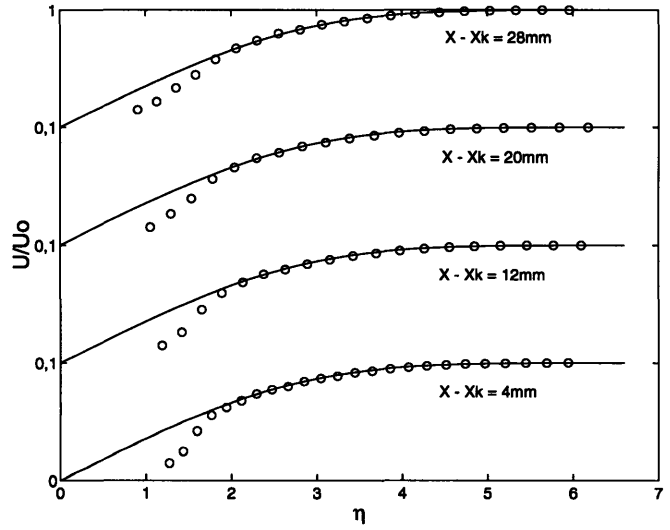

Figure 5-3: Experimental mean flow data for $R_{\delta_k^*} = 1549$ (o) and Falkner-Skan $\beta = 0.0155$ (-), $U_o = 12.5m/s$, $R_{\delta^*} = 1552$, 1558, 1564, and 1570. Edge of roughness located at $\eta = 1.075$.

difficulty which existed in shifting the previous profiles was not experienced here. The important feature of these results is the inflected profile as was observed by Klebanoff and Tidstrom [9]. The profile has little time to relax prior to transition as growth of the instability dominates the viscous forces acting to restore the flow.

5.2.2 Velocity Spectra

The mean flow distortion observed in the velocity profiles makes the flow unstable to high frequencies, causing broad-band amplification of these frequencies rather than the selective amplification of small bands predicted by linear stability theory. This nonlinear effect can be seen in the following velocity spectra results.

Velocity spectra were measured for a Reynolds number of $R_{\delta_k^*} = 927$ with the roughness located at $x = 0.37m$ corresponding to the center of the roughness arrays investigated earlier. A roughness height of $k = 0.72mm$ gave $k/\delta_k^* = 0.64$ at this Reynolds number. Measurements were taken downstream of the roughness element every $0.010m$ between $R_{\delta^*} = 942$ and $R_{\delta^*} = 1059$. Beyond this Reynolds number,

spacing increased to $50mm$ until transition occurred. Resulting spectra are shown in Figure 5-4.

Figure 5-4a contains selected spectra immediately downstream of the roughness from $R_{\delta^*} = 942$ to a location just prior to transition at $R_{\delta^*} = 1113$. Several spectra were excluded to provide a clearer picture of the trend in frequency amplification. There is a noticeable difference in spectra when compared to that of the roughness arrays centered at the same location. The primary distinction is the amplification of higher frequencies than those associated with T-S waves. This is in agreement with Klebanoff and Tidstrom [9] and found to be related to an increase in amplitude of the roughness element which causes mean flow distortion and allows for broad-band, high frequency amplification.

A difference in amplification of the selected frequency from the roughness array results is also observed. The disturbance amplitude at $f = 115Hz$ is approximately the same in both cases initially. However, no significant amplification of this frequency occurs prior to transition for the single-element roughness as it does for the small amplitude array. This is possibly due to the change in stability characteristics where $F = 70$ is no longer amplified.

Measurements immediately downstream of the roughness reveal a band of amplified frequencies centered near $700Hz$ which disappears downstream. This frequency was used to calculate the Strouhal number from $S = f_s D/U$ where f_s is the vortex shedding frequency of the roughness element, S is the Strouhal number, U is the velocity corresponding to the height of the roughness element, and D is the roughness height [1]. This resulted in a Strouhal number approximately equal to 0.12 which seems reasonable and would indicate that the amplified frequency band is associated with vortex shedding from the roughness element.

The saturation of a broad band centered near $250Hz$ is also observed. Spectra between $R_{\delta^*} = 979$ and $R_{\delta^*} = 1037$ in Figure 5-4b show this saturated region. This result reflects the balance between viscous forces driving the flow to a self-similar solution and growth of the instabilities. The flow is ultimately dominated by the growth of high frequencies and transition occurs by $R_{\delta^*} = 1164$. This is a 43 per-

cent reduction in Reynolds number, calculated as a deviation from the smooth plate transition Reynolds number of $R_{\delta^*} = 2051$, and within $0.21m$ of the roughness.

Changing the roughness Reynolds number, but keeping the roughness parameter k/δ_k^* constant allows an investigation of the role of viscosity in the mean flow and disturbance evolution (but not their creation). Spectra for the second roughness configuration, $R_{\delta_k^*} = 1242$, are shown in Figure 5-5. In this case the roughness amplitude is $k = 0.96mm$ and is located at $x = 0.657m$. The distance between successive measurements downstream of the roughness was $4mm$.

Results similar to those observed for the lower roughness Reynolds number are shown in Figure 5-5a. In this case the Reynolds number ranges from $R_{\delta^*} = 1243$ to 1330 where a shift from high frequencies to a lower frequency band centered near $175Hz$ is observed prior to transition. This shift occurs more quickly downstream than at the lower roughness Reynolds number.

Figure 5-5b, reveals a similar saturation region to that observed for the smaller roughness Reynolds number. However, instead of measuring almost identical spectra after the frequency peak shifted to $175Hz$, there was continued amplification of both lower and higher frequencies leading to transition. This would suggest that at this Reynolds number, the forces that act to restore the flow to the undistorted profile are unable to contain the growth of the instability. Transition occurs within $0.10m$ of the roughness and approximately 35 percent further upstream in R_{δ^*} than for the smooth plate.

A final experiment was run for $R_{\delta_k^*} = 1549$. Roughness of amplitude $k = 1.20mm$ was located at $x = 1.027m$ and measurements were taken every $4mm$ downstream of the roughness. Resulting spectra for $R_{\delta^*} = 1552$ to 1570, shown in Figure 5-6, indicate a significant effect of higher amplitude roughness on transition. An amplified band of high frequencies centered near $375Hz$ exist just prior to transition which occurs rather quickly downstream of the roughness. This rapid growth of high frequencies provides no opportunity for viscous forces to act to stabilize the flow. A transition location within $0.028m$ of the roughness was approximately 23 percent further upstream in R_{δ^*} than for the smooth plate.

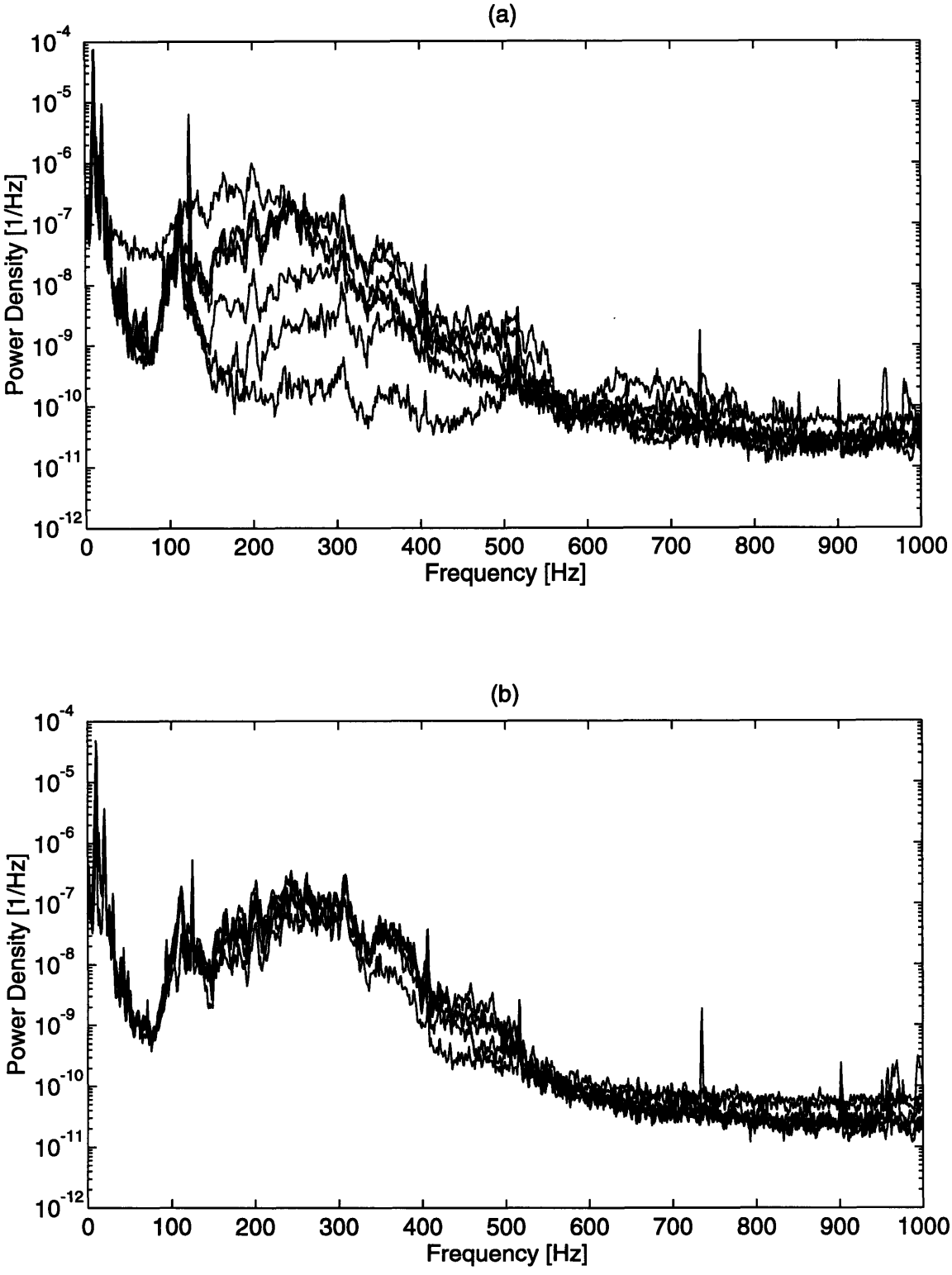

Figure 5-4: Velocity spectra for $R_{\delta_k^*} = 927$, $k = 0.72mm$, $k/\delta_k^* = 0.64$, $U/U_o = 0.15$, $U_o = 12.5m/s$. (a) $R_{\delta^*} = 942$, 955, 967, 1002, 1025, 1048, and 1113. (b) $R_{\delta^*} = 979$, 991, 1002, 1014,1025, and 1037. Power density normalized by U_o^2.

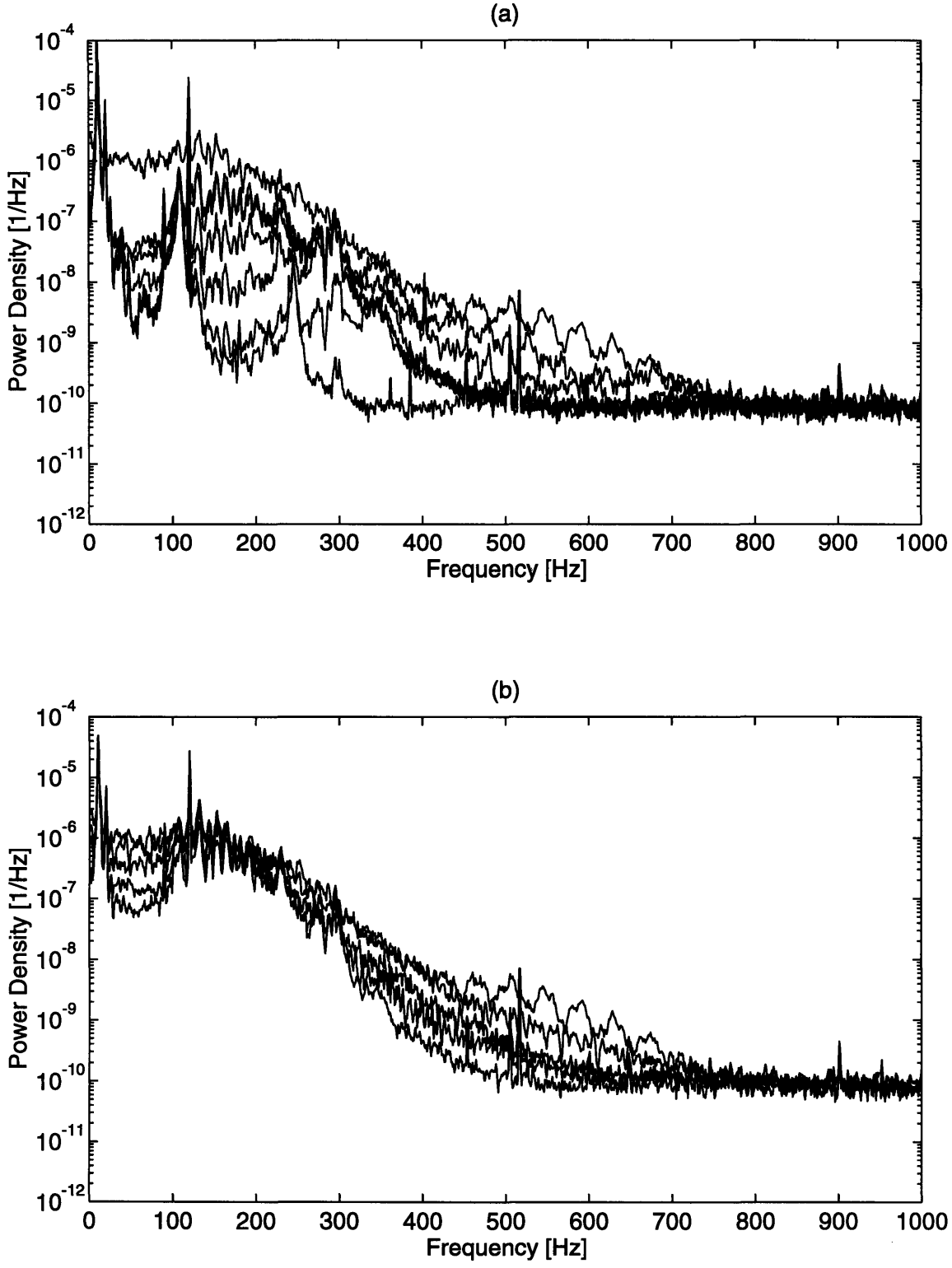

Figure 5-5: Velocity spectra for $R_{\delta_k^*} = 1242$, $k = 0.96mm$, $k/\delta_k^* = 0.64$, $U/U_o = 0.15$, $U_o = 12.5m/s$. (a) $R_{\delta^*} = 1243$, 1254, 1265, 1276, 1287, 1291, and 1330. (b) $R_{\delta^*} = 1302$, 1312, 1323, 1326, and 1330. Power density normalized by U_o^2.

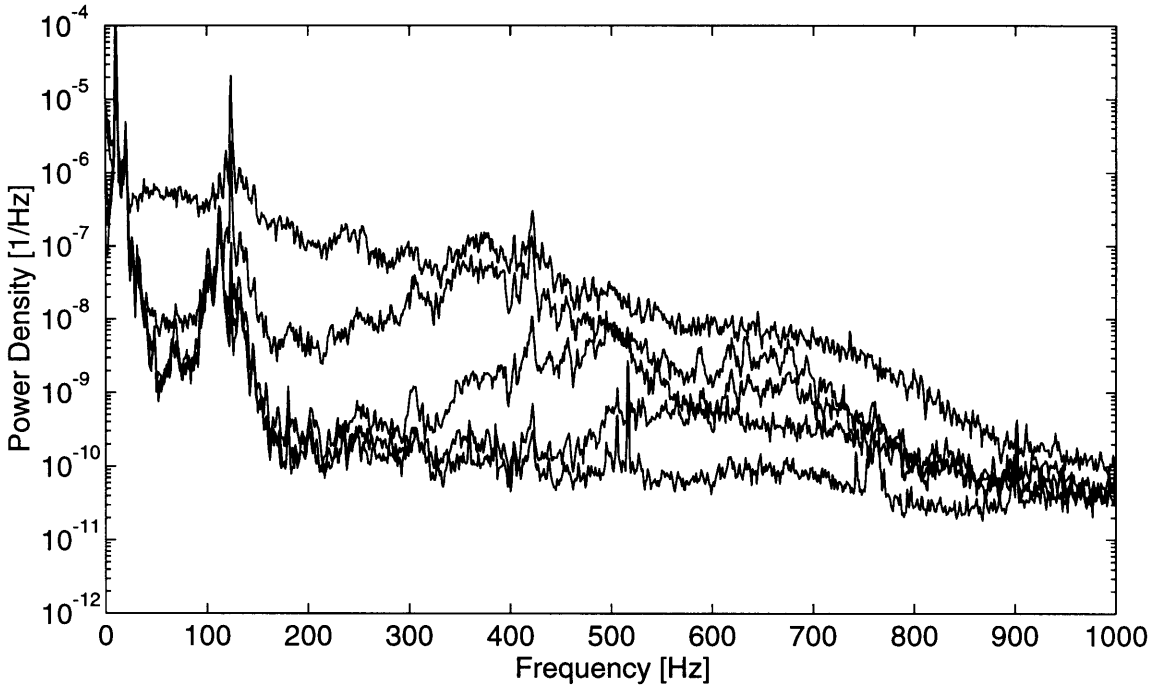

Figure 5-6: Velocity spectra for $R_{\delta_k^*} = 1549$, $k = 1.20mm$, $k/\delta_k^* = 0.64$, $U/U_o = 0.15$, $U_o = 12.5m/s$. $R_{\delta^*} = 1552$, 1555, 1558, 1567, and 1570. Power density normalized by U_o^2.

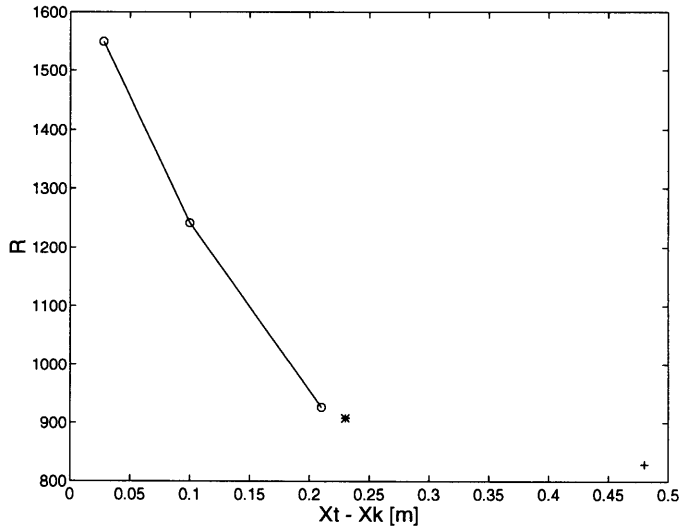

Figure 5-7: Experimental transition locations at $k/\delta_k^* = 0.64$ (o) and from Klebanoff and Tidstrom [9] experimental results at $k/\delta_k^* = 0.77$ (+) and $k/\delta_k^* = 0.86$ (∗). Reynolds number based on roughness, $R_{\delta_k^*}$.

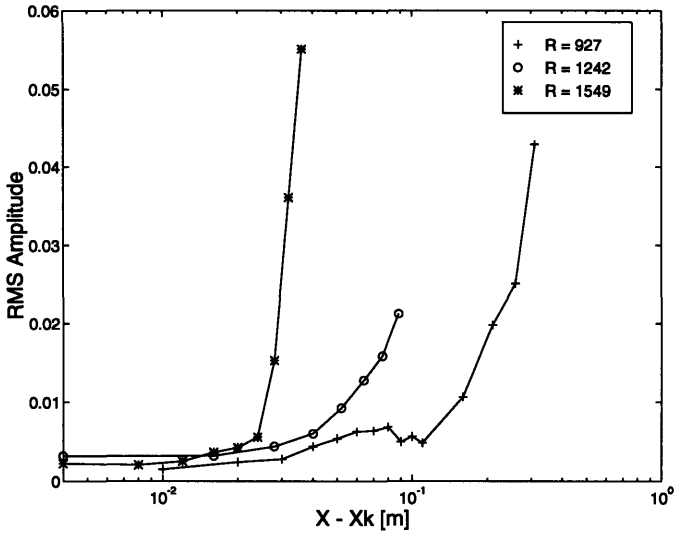

Figure 5-8: RMS amplitude of the velocity fluctuation for $R_{\delta_k^*} = 927$, 1242, and 1549 downstream of the roughness element. $U/U_o = 0.15$, $U_o = 12.5m/s$. Amplitude normalized by U_o.

Present results for $k/\delta_k^* = 0.64$ indicate that transition location relative to the leading edge occurs further downstream with an increase in roughness Reynolds number. However, the higher roughness Reynolds number promotes earlier transition in terms of the distance downstream of the roughness element as shown in Figure 5-7. Klebanoff and Tidstrom [9] results are shown in this figure for comparison at higher k/δ_k^* and lower $R_{\delta_k^*}$ and would suggest that the roughness Reynolds number has a more significant influence on transition than the roughness parameter k/δ_k^*. This is inconclusive however since the observed mean flow distortion at the lower Reynolds numbers showed some deviation from Klebanoff's results. More experiments at higher and lower roughness parameters would need to be made under the present conditions.

Growth of the disturbance amplitude downstream of the roughness element can be seen for each $R_{\delta_k^*}$ in Figure 5-8. The rate of disturbance amplification is seen to increase with an increase in $R_{\delta_k^*}$, leading to earlier transition behind the roughness. The saturation phenomenon associated with the lower roughness Reynolds numbers can also be seen in this figure, especially for $R_{\delta_k^*} = 927$.

A comparison was made of the amplification progression for three frequencies,

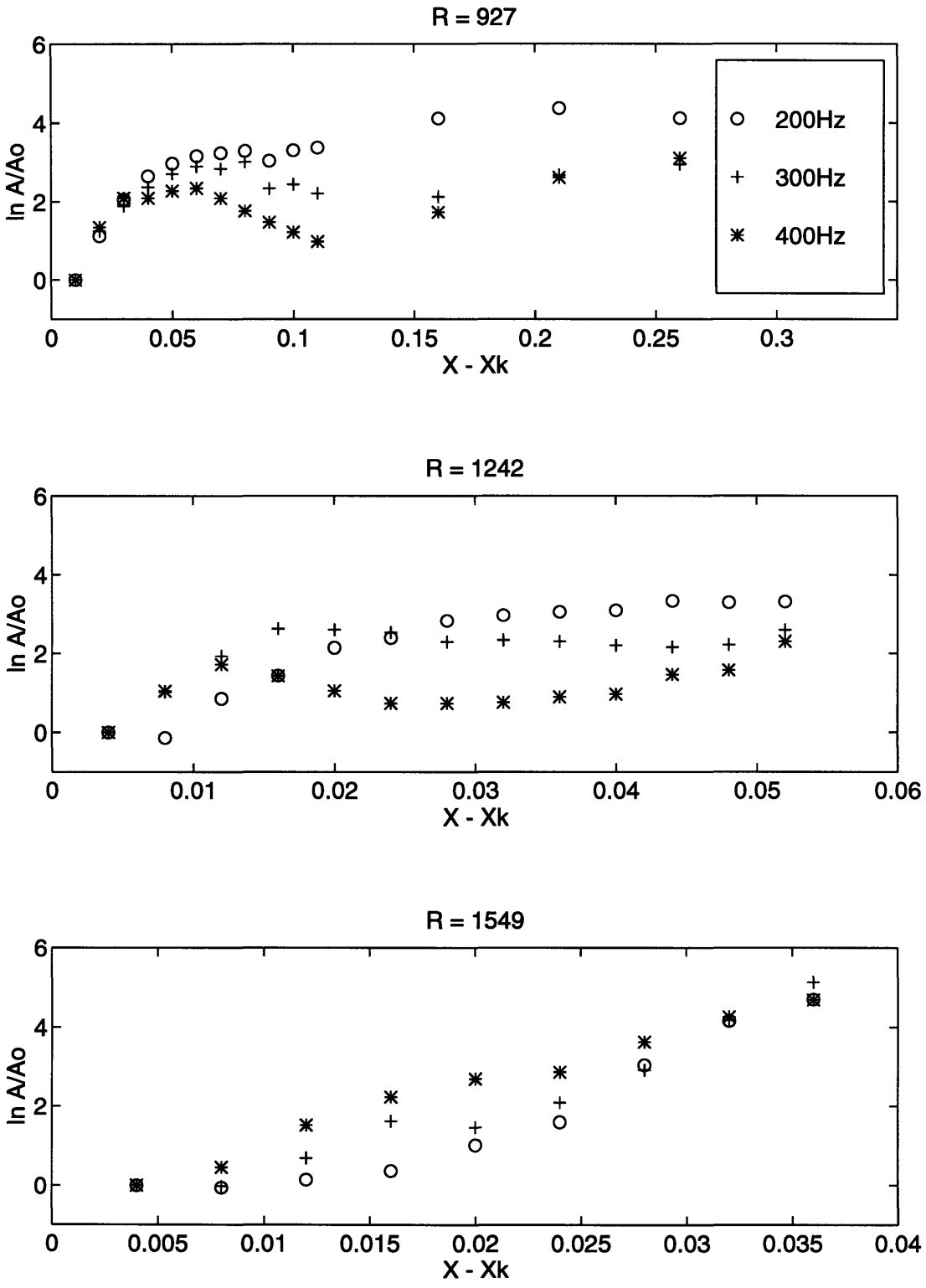

Figure 5-9: Amplification of $200Hz$, $300Hz$, and $400Hz$ downstream of the roughness element for $R_{\delta_k^*} = 927$, 1242, and 1549. $U/U_o = 0.15$, $U_o = 12.5m/s$.

$200Hz$, $300Hz$, and $400Hz$, at each $R_{\delta_k^*}$. The results are shown in Figure 5-9. For all three roughness configurations, the amplification, decay, and renewed amplification of higher frequencies is observed. It is also apparent that the dominant frequencies, those initially excited and those prior to transition, increase with increasing $R_{\delta_k^*}$.

5.3 Summary

- Single-element, 2-D roughness effects for $R_{\delta_k^*} = 927$, 1242, and 1549 at $k/\delta_k^* = 0.64$ result in mean flow distortion producing broad-band, high frequency amplification of disturbances in the boundary layer. An increase in $R_{\delta_k^*}$ results in the amplification of increasingly higher broad-band frequencies with a shift to lower frequencies as the distance downstream from the roughness element increases.

- The roughness parameter k/δ_k^* was held constant while the roughness Reynolds number was changed to observe the effect of viscosity on transition. Transition location relative to the leading edge occurs further downstream with an increase in roughness Reynolds number. The difference in Reynolds number at transition was 43, 35, and 23 percent further upstream than for the smooth plate case for $R_{\delta_k^*} = 927$, 1242, and 1549 respectively.

- An increase in roughness Reynolds number promotes earlier transition in terms of the distance downstream of the roughness element. This appears to have a greater influence on transition than the roughness parameter k/δ_k^* when compared with previous results of Klebanoff and Tidstrom [9] but is inconclusive.

- Velocity profiles for all roughness Reynolds numbers appear distorted from the Falkner-Skan solution. The lower $R_{\delta_k^*}$ results show a trend from a full to an under-developed profile as the distance from the roughness increases. However, separation was not apparent and would suggest a rapid recovery of the mean flow downstream of the roughness element.

- In the case for $R_{\delta_k^*} = 1549$, separation was apparent, resulting in clearly inflectional profiles. Rapid recovery of the mean flow does not occur suggesting that the growth of the instability constantly dominates the viscous stabilizing force attempting to restore the mean flow.

Chapter 6

Conclusions

Increased receptivity due to low amplitude roughness arrays and mean flow distortion due to larger amplitude single-element roughness were investigated. Experimental results showed evidence of enhanced receptivity for roughness array amplitudes $0.12mm \leq k \leq 0.36mm$ $(0.107 \leq k/\delta_k^* \leq 0.321)$. Mean flow distortion was also observed at these amplitudes. However, linear stability mechanisms continued to dominate the transition process. For single-element roughness amplitudes $0.72mm \leq k \leq 1.20mm$ $(k/\delta_k^* = 0.64)$, receptivity was less of an issue as mean flow distortion became the dominant factor in transition.

In the roughness array experiments, enhanced receptivity resulted from instability generation at $f = 115Hz$ which was selected as a frequency of interest in this research. The important parameters for maximizing receptivity included roughness height, location, and spacing. Disturbance amplification increased with increasing roughness height in the range of amplitudes tested. A linear relationship between roughness amplitude and disturbance amplification was shown. Location of the roughness array at branch I of the neutral stability curve and element spacing which corresponded to the selected frequency wavelength provided the mechanism for external disturbance wavelength scattering. This was necessary to generate instabilities at the desired location and frequency. Enhanced receptivity resulted in earlier transition for increasing roughness array amplitudes.

The three-element arrays produced low-amplitude instabilities which resonated

nonlinearly to produce harmonics. These harmonics are visible for all k/δ_k^* and are most prominent in spectra for $k/\delta_k^* = 0.321$. An important observation briefly addressed in the previous results is the appearance of subharmonics at $U/U_o = 0.30$. Further investigation at this boundary layer location is recommended.

Results for $k/\delta_k^* = 0.321$ in the roughness array experiments showed a trend toward amplification of higher frequencies. When the roughness parameter was increased to $k/\delta_k^* = 0.64$ in the single-element experiments, broad-band, high frequency amplification was observed. Thus the step leading to mean flow distortion as the dominant instability mechanism appears to occur between a roughness amplitude of $k = 0.36mm$ and $k = 0.72mm$.

The path to transition associated with mean flow distortion is distinctly different from the linear stability results. Amplification of frequency bands out of T-S wave range brought about transition without the selective amplification mechanism described by linear theory. Mean flow profiles for all single-element roughness amplitudes showed distortion from the theoretical Falkner-Skan profiles, especially at $k = 1.20mm$ where a clear inflection was observed.

Transition in the single-element experiments occurred at decreasing distances downstream of the roughness with an increase in R_{δ^*}. The roughness parameter $k/\delta_k^* = 0.64$ was held constant while $R_{\delta_k^*}$ was increased by increasing the roughness amplitude and moving the roughness downstream. Results suggest a Reynolds number effect on transition.

Bibliography

[1] R.D. Blevins. *Flow-Induced Vibration.* Van Nostrand Reinhold, New York, New York, 1990.

[2] K.S. Breuer. Personal communication.

[3] M. Choudhari and E.J.. Kerschen. Instability wave patterns generated by interaction of sound waves with three-dimensional wall suction or roughness. *AIAA-90-0119*, 1990.

[4] J. Cohen, K.S. Breuer, and J.H. Haritonidis. On the evolution of a wave packet in a laminar boundary layer. *J. Fluid Mech.*, 225:575–606, 1991.

[5] A.D.D. Craik. *Wave Interactions and Fluid Flows.* Cambridge University Press, Cambridge, England, 1988.

[6] J.D. Crouch. Nonlocalized receptivity of boundary layers. *J. Fluid Mech.*, 244:567–581, 1992.

[7] R. Jordinson. The flat plate boundary layer. part 1. numerical integration of the orr-sommerfeld equation. *J. Fluid Mech.*, 43(4):801–811, 1970.

[8] E.J. Kerschen. Boundary layer receptivity. *AIAA-89-1109*, 1980.

[9] P.S. Klebanoff and K.D. Tidstrom. Mechanism by which a two-dimensional roughness element induces boundary-layer transition. *Phys. Fluids*, 15(7):1173–1188, 1972.

[10] A.H. Nayfeh, S.A. Ragab, and A.A. Al-Maaitah. Effect of bulges on the stability of boundary layers. *Phys. Fluids*, 31(4):796–806, 1988.

[11] W.S. Saric, J.A. Hoos, and R.H. Radeztsky. Boundary-layer receptivity of sound with roughness. In *Proceedings of Symposium on Boundary Layer Stability and Transition to Turbulence*, Portland, Oregon, June 1991.

[12] G.B. Schubauer and H.K. Skramstad. Laminar-boundary layer oscillations and transition on a flat plate. Technical Report 909, NACA, 1948.

[13] M. Wiegel and R.W. Wlezien. Acoustic receptivity of laminar boundary layers over wavy walls. *AIAA-93-3280*, 1993.